# Translational Covariance of Flexoelectricity at Ferroelectric Domain Walls

Oswaldo Diéguez[1,2,*] and Massimiliano Stengel[3,4,†]

[1]*Department of Materials Science and Engineering, Faculty of Engineering, Tel Aviv University, Tel Aviv 6997801, Israel*

[2]*Theory and Simulation Group, Catalan Institute of Nanoscience and Nanotechnology (ICN2), CSIC, BIST, Campus UAB, Bellaterra, Barcelona 08193, Spain*

[3]*Institut de Ciència de Materials de Barcelona (ICMAB-CSIC), Campus UAB, 08193 Bellaterra, Spain*

[4]*ICREA - Institució Catalana de Recerca i Estudis Avançats, 08010 Barcelona, Spain*

(Received 1 February 2022; revised 23 May 2022; accepted 3 June 2022; published 5 July 2022)

Macroscopic descriptions of ferroelectrics have an obvious appeal in terms of efficiency and physical intuition. Their predictive power, however, has often been thwarted by the lack of a systematic procedure to extract the relevant materials parameters from the microscopics. Here we address this limitation by establishing an unambiguous two-way mapping between spatially inhomogeneous fields and discrete lattice modes. This yields a natural treatment of gradient couplings in the macroscopic regime via a long-wavelength expansion of the crystal Hamiltonian. Our analysis reveals an inherent arbitrariness in both the flexoelectric and polarization gradient coefficients, which we ascribe to a translational freedom in the definition of the polar distortion pattern. Remarkably, such arbitrariness cancels out in all physically measurable properties (relaxed atomic structure and energetics) derived from the model, pointing to a generalized translational covariance in the continuum description of inhomogeneous ferroelectric structures. We demonstrate our claims with extensive numerical tests on 180° domain walls in common ferroelectric perovskites, finding excellent agreement between the continuum model and direct first-principles calculations.

DOI: 10.1103/PhysRevX.12.031002

Subject Areas: Computational Physics
Condensed Matter Physics
Materials Science

## I. INTRODUCTION

Spatially inhomogeneous structures in ferroelectrics such as domain walls, vortices, etc., have been the subject of intense research in the past few years [1,2], because of their emerging physical properties and nontrivial topology. Considerable efforts are currently directed at identifying the physical mechanisms that govern the stability of the observed patterns and their response to external probes. In addition to the well-known factors related to the electrical and mechanical boundary conditions, flexoelectricity (describing the coupling between polarization and strain gradients [3–6]) has been receiving increasing attention in this context. On one hand, the flexoelectric coupling contributes substantially to the gradient energy, to the point that a transition to a modulated phase may occur if sufficiently strong [7–9]. On the other hand, flexoelectricity endows the spatial gradients of the main order parameters with potentially useful functionalities, e.g., a spontaneous polarization at ferroelastic twin boundaries [10,11], and a spontaneous strain at ferroelectric walls via the converse effect [12,13].

In light of these findings, improving our understanding of the interplay between flexoelectricity and ferroelectricity appears as essential for future progress. Given the advances that the first-principles theory of flexoelectricity has made since the pioneering works of Resta [14] and Hong *et al.* [15], such a goal appears now well within reach. As of early 2020, a complete calculation of the bulk flexoelectric tensor can be carried out [16,17] with the latest release of the publicly distributed ABINIT [18,19] package, providing *in principle* a solid theoretical reference for the interpretation of the experimental data [13,20]. Unfortunately, these studies have also revealed that the bulk flexoelectric coefficients are ill defined as stand-alone material properties. More specifically, their definition is plagued by two distinct ambiguities, which are respectively related to the treatment of elastic and electrostatic fields in the long-wavelength expansion [17,21,22]. This fundamental limitation prevents a straightforward comparison between theoretical and experimental

*dieguez@post.tau.ac.il
†mstengel@icmab.es

results, as further considerations are needed to make sure that the calculated values relate to what is being measured in a physically meaningful way.

If they only concerned the specifics of how the flexoelectric effect is defined and measured, these issues would be of limited importance. On the contrary, the arbitrariness of the coupling coefficients is problematic in a much broader context, as it questions the validity of the widely popular Landau-Ginzburg-Devonshire (LGD) theories of ferroelectrics, a cornerstone of the theoretical understanding of inhomogeneous polar structures for several decades. At a domain wall, standard LGD models predict [12,13] a dependence of both the energy and structure on the flexocoupling coefficient via the converse effect, which associates a uniform strain with a gradient of the polar order parameter. The obvious question is then, how can we trust such physical predictions once we know that one of the materials properties on which they depend is ill (or at least nonuniquely) defined?

To formulate the problem on firm theoretical grounds, the first challenge consists in establishing a rigorous two-way mapping between microscopic degrees of freedom and macroscopic order parameters. In the case of spatially homogeneous crystal phases, such a task poses limited conceptual issues: Building effective low-energy Hamiltonians in terms of the physically relevant lattice distortions (in perovskite crystals these typically include polarization, strain, and antiferrodistortive oxygen tilts) is now common practice [23–26] within the *ab initio* community. Whenever these degrees of freedom are no longer constant over space, however, many subtleties arise, and the partition of the energy into different macroscopic contributions generally becomes nonunique [27]. The question, then, is, are there specific criteria for ensuring that the result is physically meaningful? And, once we have solved the continuum equations, how can we verify that our solution is consistent with the "training model," i.e., our first-principles engine?

Here we show, by deriving the continuum equations and parameters via a rigorous long-wavelength approximation of the first-principles lattice Hamiltonian, that the above difficulties can be traced back to a *translational freedom* in the definition of the polar distortion pattern. As a consequence of such freedom, not only the flexocoupling $f$ but also the polarization gradient coefficient $G$ (entering the continuum functional via the squared gradient of the polarization field) is affected by an inherent arbitrariness in its definition. Crucially, we find that the respective ambiguities in $f$ and $G$ cancel out exactly in any physical prediction of the continuum model, implying that a consistent treatment of both terms is essential for the overall theory to work.

Of particular note, the aforementioned arbitrariness directly affects the definition of the elastic displacement field (and hence the strain), which we find to be nonunique. Our long-wave approach to continuum theory, however, yields unique answers for the domain-wall structure once the local field amplitudes are converted back into atomic distortions, enabling a straightforward validation of the method against direct density-functional theory (DFT) calculations. We illustrate this point by calculating 180° ferroelectric walls in six different perovskite materials, finding answers that are within 10%–20% of the "exact" result. Given the extreme (one-cell thick) abruptness of the structures, we regard this as a severe test for a continuum approach, and such an accuracy is exceptionally good. By calculating domain walls under hydrostatic pressure in $BaTiO_3$ we also demonstrate the exactness of our theory in the limit of smooth domain walls.

From our results, a new paradigm emerges in the construction of continuum models of ferroics: the invariance of the Landau-Ginzburg-Devonshire free energy with respect to a number of *generalized gauge transformations* of the parameters and fields. This implies abandoning the widespread belief that such parameters (e.g., the flexoelectric coefficient) and fields (e.g., the local strain) be well-defined physical properties of the crystal. It also emphasizes the need for an intimate connection between microscopics and macroscopics in order to achieve a qualitatively sound picture.

This work is organized as follows. In Sec. II we address the theoretical issues that arise in the design of continuum models, focusing on the aforementioned ambiguities in the definition of local strains, polar distortion patterns, and flexoelectric coefficients. In Sec. III we present our numerical tests on 180° domain walls in perovskite oxides, alongside a detailed validation against the results of direct first-principles calculations. In Sec. IV we discuss the implications of our findings in the context of the relevant literature. We summarize our work and present our conclusions in Sec. V.

## II. THEORY

### A. Statement of the problem

Consider a 180° domain wall in a ferroelectric crystal as schematically illustrated in Fig. 1. The outer extremes of both panels correspond to the oppositely oriented ferroelectric domains, where the polarization ($P$) saturates to its bulk value; in the central domain-wall region $P$ transitions from negative to positive values when moving from left to right. The atomic structure far from the wall is well described in terms of a periodically repeated crystalline cell. Such a structure can be readily obtained from a bulk calculation: one typically starts from the reference configuration, breaks the centrosymmetry by hand (e.g., by displacing atom A upward or atom O downward by a small amount), and lets the atoms relax to their polar ground state. Note that one can perform the relaxation while fixing either A or O to their original locations; while the resulting distortions $d_{A,O}$ differ [compare Figs. 1(a) and 1(b)], the

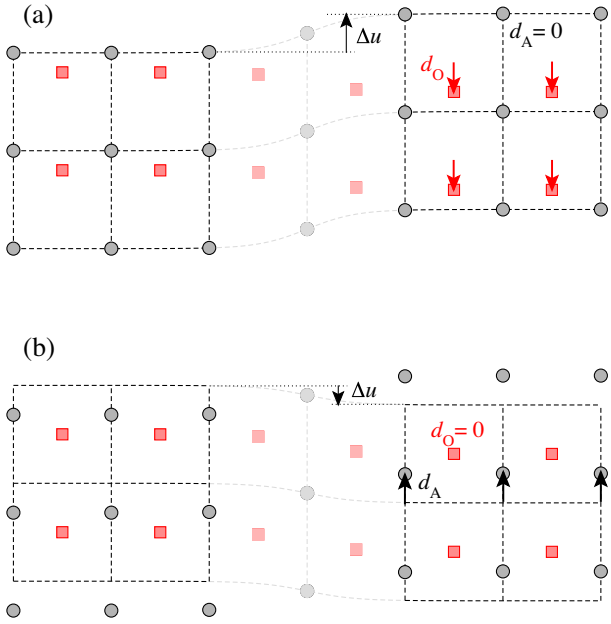


FIG. 1. Schematic model of a [100]-oriented ferroelectric domain wall in a perovskite crystal. For simplicity, only atoms in AO planes perpendicular to the wall are shown as red circles (A) and black squares (O), respectively. The elastic displacement of the crystal cells (dashed lines) is also shown. The ferroelectric distortion of the lattice deep within the domain is indicated by red and black arrows, respectively, for the displacements ($d_\kappa$) of the A and O sublattice with respect to their high-symmetry positions. The macroscopic shift of the crystal cell $\Delta u$ is also shown. Displacements are exaggerated for illustration purposes. Panels (a) and (b) illustrate how two different choices for $d_\kappa$ and $\Delta u$ can be made for the same atomic structure.

two structures are related by a rigid translation of the whole lattice, and are therefore degenerate.

Once the domain walls form, the two oppositely oriented domains no longer enjoy translational invariance separately: the wall lifts the indeterminacy modulo a rigid shift of the cell, and uniquely sets the registry between the two oppositely polarized half-lattices. The shift that we must add to the calculated bulk atomic structure to correctly align the two semi-infinite regions can conveniently be rationalized in terms of the *elastic displacement field* $u(x)$, which undergoes a jump $\Delta u$ when moving across the wall along the normal direction ($x$). Thus, the spontaneous alignment between the two domains can be understood physically as an electromechanical effect, where the elastic degrees of freedom emerge as a secondary consequence of the primary polar distortion of the lattice. And indeed, recent works [12,13] have clarified that the net elastic displacement is due to *converse flexoelectricity*, and $\Delta u$ can be related linearly to the flexocoupling coefficient(s) of the crystal in its cubic reference phase.

Earlier works, however, have overlooked the central conceptual issue with the above interpretation. Since the ferroelectric distortion pattern within the bulk domains (quantified here by $d_\kappa$, with $\kappa = \mathrm{A}, \mathrm{O}$) is ill defined, the amount of elastic displacement $\Delta u$ that we must incorporate to obtain the correct registry between the left and right half-lattices is also ill defined. This is obvious by looking at Figs. 1(a) and 1(b), where we compare two different choices for $d_\kappa$ and $\Delta u$. Clearly, the total atomic distortions within each domain, given by $\pm(d_\kappa + \Delta u/2)$, are the same in Figs. 1(a) and 1(b). And yet, what we understand as the "macroscopic elastic offset" between the domains, $\Delta u$, markedly differs. This situation is paradoxical in light of the widespread assumption that the local elastic displacement field (and hence the local strain) be a physically unambiguous degree of freedom of the crystal. The sketch of Fig. 1 seems to disprove such an interpretation. As we have anticipated in the Introduction, abandoning such a long-established paradigm brings about a number of conceptual troubles; we address them in the remainder of this work.

### B. Macroscopic theory

To frame our discussion, in this section we recap the established [12] macroscopic theory for an Ising-like 180° ferroelectric domain wall as illustrated in Fig. 1. For simplicity, we shall exclusively focus on the transverse ($y$) component of the polarization: Longitudinal ($x$) components are typically small in perovskite ferroelectrics, and would require an explicit treatment of the electrostatic energy, which is nontrivial in the flexoelectric case [27]. We also restrict our attention to a single strain component, the $xy$ shear, which is the most relevant one to our present scope. (This implies neglecting the tetragonal distortion of the crystal cells deep within the domains.) Within these assumptions, the simplest free-energy functional to describe the problem is

$$F(P,\varepsilon) = \frac{C}{2}\varepsilon^2 + \frac{A}{2}P^2 + \frac{B}{4}P^4 + f\varepsilon\frac{\partial P}{\partial x} + \frac{G}{2}\left(\frac{\partial P}{\partial x}\right)^2. \quad (1)$$

Here $P$ is the parallel ($y$) component of the polarization, while the normal to the wall is indicated as $x$;

$$\varepsilon = \frac{\partial u}{\partial x} \quad (2)$$

is the shear ($xy$) component of the strain, defined as the $x$ derivative of the parallel ($y$) component of the displacement field $u$, $C$ is the elastic constant ($C_{44}$ component), $A$ and $B$ are the standard parameters of the homogeneous Landau potential, $f$ is the flexocoupling coefficient, and $G$ is the polarization gradient coefficient. Note that the flexoelectric coupling is written here in terms of the converse effect (uniform strain in response to a $P$ gradient); it is related to the direct effect and to the standard Lifshitz-invariant formula via simple integrations by parts:

$$f\varepsilon\frac{\partial P}{\partial x} \simeq -f\frac{\partial \varepsilon}{\partial x}P \simeq \frac{f}{2}\left(\varepsilon\frac{\partial P}{\partial x} - \frac{\partial \varepsilon}{\partial x}P\right). \tag{3}$$

(The difference between the three expressions consists in surface terms, irrelevant for the present bulk theory.)

By imposing the stationary condition,

$$\frac{\partial F}{\partial \varepsilon} = 0, \tag{4}$$

the strain can be integrated out, which immediately leads to the following result [12]:

$$\varepsilon = -\frac{f}{C}\frac{\partial P}{\partial x} \rightarrow u = -\frac{f}{C}P. \tag{5}$$

(We have eliminated a trivial integration constant in $u$ by imposing that $u$ vanishes whenever $P = 0$.) Therefore, the displacement field at a ferroelectric domain wall adopts the exact same spatial profile as the polarization, except for the $-f/C$ scaling factor. From Eq. (5) one then can extract the net elastic offset $\Delta u$ that we introduced in the previous section:

$$\Delta u = -2\frac{P_0 f}{C}. \tag{6}$$

After eliminating the strain, we obtain the following simpler expression for the free energy:

$$F(P) = \frac{A}{2}P^2 + \frac{B}{4}P^4 + \frac{\tilde{G}}{2}\left(\frac{\partial P}{\partial x}\right)^2, \quad \tilde{G} = G - \frac{f^2}{C}. \tag{7}$$

The condition for stability is that the renormalized polarization gradient coefficient be positive, $GC > f^2$. (This criterion is well known: if $f$ is large enough, the system becomes unstable and an incommensurate transition to a modulated state may occur [7–9].) The equation of state is given by the stationary condition with respect to $P$:

$$AP + BP^3 - \tilde{G}\frac{\partial^2 P}{\partial x^2} = 0. \tag{8}$$

We shall attempt a trial solution of the type

$$P(x) = P_0 \tanh\left(\frac{x}{\xi}\right). \tag{9}$$

After a few steps of straightforward algebra, we arrive at

$$P_0^2 = -\frac{A}{B}, \qquad \xi^2 = \frac{2\tilde{G}}{|A|}. \tag{10}$$

$P_0$ is determined by the bulk Landau potential, while $\xi$ is a length, and has the obvious physical meaning of domain-wall thickness.

The domain-wall energy per unit area can be obtained by integrating the free-energy density along the normal to the wall,

$$W = \int dx[F(P(x)) - F_0], \tag{11}$$

where $F_0$ is the energy density of the monodomain ground state. One arrives at

$$W = \frac{A^2}{2B}\xi\int_{-\infty}^{+\infty} dx\,\mathrm{sech}^4(x) = \frac{A^2}{2B}\xi\frac{4}{3} = \frac{8}{3}|F_0|\xi, \tag{12}$$

where $F_0 = -A^2/4B$ is the bulk energy density. [Since $F_0$ is an energy per unit volume, Eq. (12) correctly describes $W$ in units of energy per length squared].

An interesting consequence of the above derivations is that the main physical properties of the wall (the thickness $\xi$ and the energy $W$) depend on the inhomogeneous coefficients only via the renormalized gradient coupling $\tilde{G}$, while other features (the elastic offset $\Delta u$) explicitly depend on the flexocoupling $f$. This means that we can replace $f$ and $G$ with arbitrary numbers, provided that $G - f^2/C$ retains the original value, and extract the same physical answers for $\xi$ and $W$; $\Delta u$, on the other hand, is not invariant with respect to such a transformation. This property of Eq. (1) may appear at first sight as a mathematical curiosity, but has profound physical implications in relation to the paradox illustrated in Fig. 1; we explore them in the following sections.

### C. Direct mapping to the microscopics

To test the validity of Eq. (1) in real systems, we need to establish a microscopic interpretation of the order parameters entering the continuum functional. In full generality, we use the following two-step procedure. First, we express the individual atomic displacements as continuum functions of the real-space coordinates $\mathbf{r}$ via a linear transformation of the relevant vector fields $v_{\nu\beta}(\mathbf{r})$:

$$u_{\kappa\alpha}(\mathbf{r}) = \sum_{\nu\beta} v_{\nu\beta}(\mathbf{r})T_{\nu\beta,\kappa\alpha}. \tag{13}$$

($T_{\nu\beta,\kappa\alpha}$ is the transformation matrix of the mapping, describing the displacement of the sublattice $\kappa$ along $\alpha$ for a unit amplitude of $v_{\nu\beta}$, where $\beta$ runs over the Cartesian components of the vector field $\mathbf{v}_\nu$.) Second, we write the displacement of the atom in the $l$th cell by sampling the atomic displacement fields at the undistorted lattice sites $\mathbf{R}_{l\kappa}^{(0)}$:

$$u_{\kappa\alpha}^l = u_{\kappa\alpha}(\mathbf{R}_{l\kappa}^{(0)}). \tag{14}$$

The combination of Eqs. (13) and (14) endows the order parameters with the meaning of envelope functions,

generally smooth on the scale of the interatomic spacings, that modulate a cell-periodic displacement pattern of the atoms over the volume of the crystal.

We assume a perovskite-structure lattice henceforth and focus on two specific order parameters, $\nu = u$, $P$, corresponding to the elastic displacement and ferroelectric polarization. We identify their respective blocks of the transformation matrix $\mathbf{T}$ with the threefold degenerate acoustic and "soft" transverse modes of the undistorted cubic structure at the zone center. Within the standard choice of the coordinate axes, both blocks are diagonal on the Cartesian indices,

$$T_{u\beta,\kappa\alpha} = u_\kappa^{(\beta)}\delta_{\alpha\beta}, \qquad T_{P\beta,\kappa\alpha} = p_\kappa^{(\beta)}\delta_{\alpha\beta}. \tag{15}$$

$u_\kappa^{(\beta)}$ and $p_\kappa^{(\beta)}$ are sets of three five-dimensional *basis vectors*, each forming a $T_{1u}$ irreducible representation of the $Pm\bar{3}m$ point group. Regardless of the microscopics, $u_\kappa^{(\beta)}$ depends neither on the sublattice index $\kappa$ nor on the Cartesian index $\beta$, as it describes a rigid shift of the cell that is collinear with $u_\beta$ [27]:

$$u_\kappa^{(\beta)} = 1. \tag{16}$$

Equation (13) reduces then to the following simplified expression,

$$u_{\kappa\alpha}(\mathbf{r}) = u_\alpha(\mathbf{r}) + P_\alpha(\mathbf{r})p_\kappa^{(\alpha)}, \tag{17}$$

where the only remaining task consists in specifying $p_\kappa^{(\alpha)}$.

As detailed in Sec. II F, we require that the homogeneous solution of the Landau potential, Eq. (1), reproduce the spontaneous bulk ferroelectric distortion pattern $d_\kappa^{(\beta)}$ via Eq. (17):

$$d_\kappa^{(\beta)} = P_0 p_\kappa^{(\beta)}. \tag{18}$$

This condition implies that $p_\kappa^{(\beta)}$ has four independent entries and depends on $\beta$ by a permutation of the oxygen indices [21]. Equation (18) does not lead to a unique solution for $p_\kappa^{(\beta)}$, though: (i) There is a (trivial) freedom in the choice of the unit in which both $\mathbf{P}(\mathbf{r})$ and $p_\kappa^{(\beta)}$ are expressed, and (ii) because of the translational invariance that we have mentioned earlier, $d_\kappa^{(\beta)}$ is only defined modulo an arbirary shift of the whole lattice. In the following, we assume that some choice has been made for (i) and (ii) and proceed to deriving all the coefficients entering Eq. (1) in terms of microscopic quantities; later on, we discuss the implications of (ii) in regards to the apparent paradox of Fig. 1.

### D. Calculation of the coupling coefficients

The homogeneous coefficients $A$ and $B$ are easy to extract from a first-principles calculation: they are readily given by a quartic fit of the energy of the primitive cell as a function of the distortion amplitude along the direction (in configuration space) spanned by $p_\kappa^{(\beta)}$. The gradient terms (especially $f$ and $G$) are technically more challenging to calculate, in that they are defined in terms of spatially modulated (and hence non-cell-periodic) atomic distortion patterns. Recent developments [16,22,27] in density-functional perturbation theory have overcome these difficulties by applying the long-wavelength method to the phonon problem. We show in the following that Eq. (13) directly connects to the formalism of Refs. [22,27], and hence leads to a physically sound definition of $C$, $f$, and $G$.

Since all gradient terms are harmonic, we consider a linear-response regime in the field amplitude with respect to the high-symmetry cubic phase. To capture the spatial modulation, it is convenient to work in Fourier space and express the relevant perturbations of the continuum fields as a constant times a complex phase, e.g., $\mathbf{P}(\mathbf{r}) = \mathbf{P}^{\mathbf{q}}e^{i\mathbf{q}\cdot\mathbf{r}}$. Via Eq. (14), the corresponding lattice distortions can be written as linear combinations of monochromatic displacement patterns of the atoms:

$$u_{\kappa\alpha}^{l} = u_{\kappa\alpha}^{\mathbf{q}} e^{i\mathbf{q}\cdot\mathbf{R}_{l\kappa}^{(0)}}. \tag{19}$$

The second derivatives of the energy with respect to $u_{\kappa\alpha}^{\mathbf{q}}$ define [22] the *force-constants matrix* at the specified wave vector $\mathbf{q}$,

$$\Phi_{\kappa\alpha,\kappa'\beta}^{\mathbf{q}} = \frac{\partial^2 E}{\partial u_{\kappa\alpha}^{-\mathbf{q}} \partial u_{\kappa'\beta}^{\mathbf{q}}}, \tag{20}$$

which provides the formal link to the established density-functional perturbation theory framework [22].

The macroscopic limit of Eq. (20) is taken via a long-wave expansion [17,22] in powers of $\mathbf{q}$:

$$\Phi_{\kappa\alpha,\kappa'\beta}^{\mathbf{q}} = \Phi_{\kappa\alpha,\kappa'\beta}^{(0)} - iq_\gamma \Phi_{\kappa\alpha,\kappa'\beta}^{(1,\gamma)} - \frac{q_\gamma q_\delta}{2}\Phi_{\kappa\alpha,\kappa'\beta}^{(2,\gamma\delta)} + \cdots. \tag{21}$$

The zeroth order term is the usual zone-center force-constants matrix in short-circuit electrical boundary conditions. (It may be used to compute the homogeneous quadratic coefficient $A$.) The first-order term vanishes in the cubic perovskite reference structure. Finally, the second-order term allows one to extract the sought-after information about flexoelectricity, polarization gradient, and elasticity via a projection onto the elastic and polar displacement patterns. In particular, in our specific context of the [100]-oriented wall with the polarization oriented along [010], Eqs. (16) and (15) lead to the following explicit formulas,

$$C = -\frac{1}{2\Omega}\sum_{\kappa\kappa'}\Phi^{(2,xx)}_{\kappa y,\kappa' y}, \tag{22a}$$

$$f = -\frac{1}{2\Omega}\sum_{\kappa\kappa'}\Phi^{(2,xx)}_{\kappa y,\kappa' y}p^{(y)}_{\kappa'}, \tag{22b}$$

$$G = -\frac{1}{2\Omega}\sum_{\kappa\kappa'}\Phi^{(2,xx)}_{\kappa y,\kappa' y}p^{(y)}_{\kappa}p^{(y)}_{\kappa'}, \tag{22c}$$

where $\Omega$ is the volume of the undistorted primitive cell.

To connect with the existing first-principles theory of flexoelectricity, it is useful to recall the definition [17,22] of the *force-response coefficient*,

$$f^{\kappa'} = -\frac{1}{2}\sum_{\kappa}\Phi^{(2,xx)}_{\kappa y,\kappa' y}, \tag{23}$$

as the force on the sublattice $\kappa'$ produced by a gradient of the shear strain. A comparison between Eqs. (22) and (23) shows that the flexocoupling coefficient is properly defined here as the geometrical force on the polar mode produced by a strain gradient, $f = \sum_{\kappa'} f^{\kappa'} p^{(y)}_{\kappa'}/\Omega$, consistent with earlier works [27,28]. Also, the definition of the elastic constant $C$ is consistent with the classic result of Born and Huang [29], as revisited recently in a modern electronic-structure context [17,22]. Note that $f^{\kappa}$ and $C$ comply with the "elastic sum rule" [17,22],

$$C = \frac{1}{\Omega}\sum_{\kappa'} f^{\kappa'}, \tag{24}$$

as can be easily verified via Eq. (22).

The fact that we obtain the elastic tensor, which is usually regarded as a homogeneous coupling parameter, via a similar procedure as spatial dispersion coefficients such as $G$ and $f$, might come as a surprise. This is justified by the fact that a uniform strain is a *gradient* of the elastic displacement field, and therefore it formally enters the long-wave expansion of the dynamical matrix on the same footing as a gradient of the polar mode: elasticity, flexoelectricity, and polarization gradient coupling all occur at second order in the wave vector $\mathbf{q}$.

### E. Covariance principle

As expressed via Eqs. (22), it might appear that the three dispersion coefficients $C$, $f$, and $G$ are well-defined (and measurable) physical properties of the crystal; most authors have indeed used such an assumption in the past, either implicitly or explicitly. And yet, while $C$ is indeed a well-defined crystal property, neither $f$ (as pointed out in earlier works [21]) nor $G$ (as we demonstrate in the following) are; on the contrary, they both suffer from an unavoidable arbitrariness. We anticipate that their ambiguity is *physical*, i.e., it is not specific to the method one uses to calculate the coefficients within microscopic theory, and is directly related to the paradox of Fig. 1.

After a quick glance at Eq. (22), it is not difficult to see where this arbitrariness may come from. Of the two ingredients that enter the definition of $C$, $f$, and $G$, the $\Phi^{(2,xx)}$ matrix is well defined, as it directly emerges from a long-wave expansion of the force constants. As we have anticipated earlier, however, the basis vector $p^{(y)}_{\kappa}$ is only defined modulo a rigid displacement of the whole lattice (Fig. 1). In other words, we can always replace $p^{(y)}_{\kappa}$ with any vector that differs from $p^{(y)}_{\kappa}$ by a $\kappa$-independent constant. There is no fundamental symmetry principle that favors one choice over the other—it is entirely a matter of convention. Let us see what happens if we operate such a transformation, by defining a new basis vector as

$$p^{(y)\prime}_{\kappa} = p^{(y)}_{\kappa} + \lambda. \tag{25}$$

Evidently, the homogeneous coupling coefficients are unaffected, since the energetics of the uniform phase is insensitive to the choice of the origin. This is not the case for the gradient coefficients, whose transformation rules can be straightforwardly derived by plugging Eq. (25) into Eq. (22):

$$f' = f + \lambda C, \tag{26a}$$

$$G' = G + 2\lambda f + \lambda^2 C. \tag{26b}$$

The fact that both the flexoelectric and gradient coefficients depend on an arbitrary constant $\lambda$ is actually easy to rationalize on elementary physical grounds. Introducing a shift in the polar distortion is harmless in the homogeneous case, but the gradient of $P$ comes with an extra strain field, which contributes to both the elastic and flexoelectric terms in the free energy.

One might wonder, at this point, whether Eq. (1) can be trusted at all, given the aforementioned arbitrariness. To answer this question, it is useful to understand the impact of Eqs. (25) and (26) on the domain-wall solution. Crucially, the renormalized gradient coefficient $\tilde{G}$ remains unchanged,

$$\tilde{G}' = \tilde{G}, \tag{27}$$

as the respective $\lambda$-dependent contributions to $f$ and $G$ exactly cancel out. This means that all *physically measurable* properties of the domain wall, i.e., the thickness $\xi$ and the energy $W$, are well defined regardless of the specific convention that we choose for $p^{(y)}_{\kappa}$; the equilibrium solution for $P(x)$ is also unaffected. The only feature that changes with $\lambda$ is the equilibrium solution for the elastic displacement field, and hence the *local strain*,

$$u'(x) = -\frac{f'}{C}P(x) = u(x) - \lambda P(x). \tag{28}$$

This result looks, at first sight, surprising: by modifying the definition of the polar distortion we have obtained the same profile for $P(x)$, exactly the same energy, but a different solution for the strain field. The solution to this puzzle resides in Eq. (14), which is our gateway from the continuum solution back to the microscopics. And indeed, one can quickly verify that the change in the strain field exactly cancels out with the change in the displacements that are associated with the redefinition of $p_\kappa^{(y)}$, leaving the equilibrium solution for the individual atomic displacements well defined (that is, $\lambda$ independent) and unique. This provides, in a nutshell, the solution to the paradox of Fig. 1, and constitutes one of our main formal results.

That Eq. (1) behaves this way is not a coincidence, but rather the consequence of a more general *covariance principle*. Suppose we operate the following transformation of the fields and the distortion vectors,

$$p_\kappa^{(\alpha)\prime} = p_\kappa^{(\alpha)} + \lambda, \tag{29a}$$

$$\mathbf{u}'(\mathbf{r}) = \mathbf{u}(\mathbf{r}) - \lambda \mathbf{P}(\mathbf{r}), \tag{29b}$$

where $\lambda$ is an arbitrary dimensionless scalar. The atomic distortions associated with the displacement and polarization fields via Eq. (17) are manifestly invariant with respect to Eq. (29). This means that the original and primed quantities refer to the same configuration of the system; i.e., they are physically equivalent macroscopic representations of the same distorted crystal structure. It is natural then to require *a priori* from any continuum functional of $\mathbf{u}$ and $\mathbf{P}$ to be covariant with respect to the choice of $\lambda$, i.e., that it transforms as Eq. (29). The results of this section demonstrate that Eq. (1) complies with such a requirement, provided that both flexoelectricity and polarization gradient coefficients are consistently calculated.

### F. Converse mapping to the continuum fields

It is ironic, in light of these results, to realize that macroscopic theory is far better suited to predicting equilibrium atomic positions rather than "traditional" macroscopic quantities, such as the strain. To rationalize such an outcome, and get convinced that "it cannot be otherwise," it is illuminating to consider the *converse* mapping between continuum fields and microscopics, i.e., the procedure that allows one to extract the values of $\mathbf{P}(\mathbf{r})$ and $\mathbf{u}(\mathbf{r})$ given a distorted configuration of the crystal. We shall follow the same two-step procedure as in Sec. II C, but taken in reverse order: (i) transform the discrete sublattice distortions into continuum functions of all space, (ii) perform a local projection of the individual atomic displacements onto the subspace spanned by the active lattice modes, i.e., those associated to the fields $\mathbf{v}_\nu(\mathbf{r})$ via the transformation matrix $\mathbf{T}$.

Step (i) does not involve any ambiguity as long as the atomic displacement pattern is mesoscopic in nature (i.e., the distortion amplitudes vary on a length scale that is much larger than the interatomic spacings). Such an assumption implies that, if we express the distortion in reciprocal space, all phonon amplitudes $u_{\kappa\alpha}(\mathbf{q})$ vanish at the zone boundary. This is a sufficient condition for the Fourier continuation of the atomic displacements from discrete to continuum,

$$u^l_{\kappa\alpha} = u_{\kappa\alpha}(\mathbf{R}^{(0)}_{l\kappa}) \to u_{\kappa\alpha}(\mathbf{r}), \tag{30}$$

to be uniquely defined [27]. (Whenever the above condition breaks down one can still extract continuum fields from the atomistics by applying standard "macroscopic averaging" [30,31] techniques).

Regarding step (ii), we shall define the continuum fields by inverting Eq. (13),

$$v_{\nu\beta}(\mathbf{r}) = \sum_{\kappa\alpha} u_{\kappa\alpha}(\mathbf{r})\tilde{T}_{\kappa\alpha,\nu\beta}, \tag{31}$$

where $\tilde{T}_{\kappa\alpha,\nu\beta}$ is the converse transformation matrix, which satisfies the condition $\tilde{\mathbf{T}}\mathbf{T} = \mathbf{I}$. Similarly to the direct one, $\tilde{\mathbf{T}}$ is diagonal on the Cartesian indices, $\tilde{T}_{\kappa\alpha,\nu\beta} = \delta_{\alpha\beta}\tilde{T}_{\kappa\alpha,\nu\alpha}$. The columns referring to $\nu = u$, $P$, which we indicate as $\tilde{u}_\kappa^{(\alpha)} = \tilde{T}_{\kappa\alpha,u\alpha}$ and $\tilde{p}_\kappa^{(\alpha)} = \tilde{T}_{\kappa\alpha,P\alpha}$, are the *duals* to the direct basis vectors, respectively, $u_\kappa^{(\beta)}$ and $p_\kappa^{(\beta)}$, that we introduced in Sec. II C. The basic requirement on the direct and dual vectors is that they form an orthonormal set:

$$\begin{aligned}\sum_\kappa \tilde{u}_\kappa^{(\alpha)} u_\kappa^{(\beta)} &= \sum_\kappa \tilde{p}_\kappa^{(\alpha)} p_\kappa^{(\beta)} = \delta_{\alpha\beta},\\ \sum_\kappa \tilde{u}_\kappa^{(\alpha)} p_\kappa^{(\beta)} &= \sum_\kappa \tilde{p}_\kappa^{(\alpha)} u_\kappa^{(\beta)} = 0.\end{aligned} \tag{32}$$

This is a necessary condition to ensure consistency, e.g., that a subsequent application of the direct and converse mapping recovers the initial values of the continuum fields. The most general choice that satisfies these constraints consists in introducing a set of sublattice-dependent weights $w_\kappa$ whose sum is unity, $\sum_\kappa w_\kappa = 1$. Then, we define the duals as

$$\tilde{u}_\kappa^{(\beta)} = w_\kappa, \tag{33a}$$

$$\tilde{p}_\kappa^{(\beta)} = w_\kappa p_\kappa^{(\beta)}. \tag{33b}$$

This way, the orthonormality of the elastic displacement vectors is enforced by construction, while the remainder of Eq. (32) leads to the following two conditions on $p_\kappa^{(\beta)}$:

$$\sum_\kappa w_\kappa p_\kappa^{(\beta)} = 0, \tag{34a}$$

$$\sum_\kappa w_\kappa [p_\kappa^{(\beta)}]^2 = 1. \tag{34b}$$

Equation (34a) is a "hard" requirement on $p_\kappa$, and must always be enforced after some choice of weights is made. This condition lifts the indeterminacy of the polar distortion vector that we illustrated in Fig. 1, and clarifies the role of $w_\kappa$ in subtracting the (weighted) average displacement of the cell from the polar mode. Doing so is consistent with physical intuition: the polarization, by its nature, is a distortion of the lattice that does not move the unit cell of the crystal as a whole. Thus, the translational freedom that we have described in the earlier sections can be equivalently expressed as a *weight freedom* in the converse mapping to the macroscopics, which provides an even more direct connection to the theory of Ref. [21].

Equation (34b), on the other hand, is a consequence of Eq. (33b), which is to some extent arbitrary. Indeed, one can always multiply Eq. (34b) by a constant factor; such freedom has to do with the choice of units that we use to measure the polar distortion amplitude. (For example, one could require $P_0$ to coincide with the spontaneous polarization of the ferroelectric crystal, as customary in macroscopic theories.) The present convention, which consists in measuring $P(x)$ in length units, has the drawback that the normalization condition [Eq. (34b)], and hence the values of all coefficients of Eq. (1), depends on the choice of weights. Still, we prefer it here because it bears a direct formal link to the eigenvectors of the dynamical matrix (see Appendix A), and for consistency with earlier works [10,27,28].

Equations (34a) and (34b), together with the prescriptions of Sec. II C, yield a well-defined procedure to construct the eigendisplacement vectors, and hence the model parameters, given a set of weights $w_\kappa$. Starting from the atomic distortions in the relaxed ferroelectric structure with the polarization oriented along $\beta$, $d_\kappa^{(\beta)}$, we first of all enforce Eq. (34) via

$$\bar{d}_\kappa^{(\beta)} = d_\kappa^{(\beta)} - \sum_\kappa w_\kappa d_\kappa^{(\beta)}. \tag{35}$$

Then, we define the amplitude of the spontaneous distortion as

$$P_0 = \sqrt{\sum_\kappa w_\kappa [\bar{d}_\kappa^{(\beta)}]^2}. \tag{36}$$

Finally, we enforce Eq. (34b) by defining the dimensionless eigendisplacement vector as $p_\kappa^{(\beta)} = \bar{d}_\kappa^{(\beta)}/P_0$.

### G. Arbitrariness of the strain field

With the above derivations, we have established the continuum displacement field as a weighted average over all sublattices:

$$\mathbf{u}(\mathbf{r}) = \sum_\kappa w_\kappa \mathbf{u}_\kappa(\mathbf{r}). \tag{37}$$

The issue with this formula, which is otherwise rather trivial, is the fact that the weights are completely arbitrary. There may be, of course, some choices that are preferable over others, for different reasons. Several authors [13,27], for example, advocate the use of the physical masses of the atoms as weights; this is convenient for dynamical problems, where masses indeed play a role, and provides the physically intuitive interpretation of the displacement field as the displacement of the local center of mass. Then, microscopists routinely use the positions of the heaviest ions to define the local strain, as they correspond to the brightest spots in the images; this implies setting their weight to unity, and the others to zero. Simply taking the average displacement of the cell (with equal weights) is not uncommon, either.

The key point is that there is no *fundamentally* right (or wrong) choice: since spatial inversion is broken in the polar structure, within the bulk domains the relation between the cell origin and the atomic positions cannot be fixed by symmetry (see Fig. 1). Yet, the "covariance" of Eq. (1) with respect to the weight arbitrariness guarantees that the physics is uniquely described, even if the strain field (and hence the net elastic offset across the wall, $\Delta u$) depends on such choice. Note that this result, which has been established here for a static domain-wall structure, holds in full generality: In Appendix B we generalize it to the time-dependent regime, and use it to reconcile the existing controversies around the so-called "dynamical flexoelectric effect."

An important consequence of the formalism developed here is that the definitions of strain and polarization are intimately related: they are both bound, respectively, via Eqs. (37) and (34), to the same weight choice ambiguity. And indeed, Eq. (29) shows that $\mathbf{u}(\mathbf{r})$ is ambiguous only in the presence of a spatially nonuniform polarization, and is uniquely defined otherwise. To see this, recall that the strain is defined as the first gradient of the displacement field. If $\mathbf{P}(\mathbf{r})$ vanishes or is constant over space, Eq. (29) yields $\partial u_\alpha/\partial r_\beta = \partial u'_\alpha/\partial r_\beta$, independent of $\lambda$; i.e., the strain becomes a well-defined quantity. This is manifestly consistent with Eq. (37): if all the $\mathbf{u}_\kappa(\mathbf{r})$ are equal modulo a constant (which is true if the polarization is uniform), their spatial gradients coincide; then, any choice of the weights yields the same result for the strain.

We have achieved, therefore, a complete physical picture. There are three, at first sight unrelated, ambiguities in the mapping from continuum to atomistics and vice versa,

and concern (i) the definition of the local strain, (ii) the definition of the polar distortion, and (iii) the definition of the flexocoupling and gradient coefficients in the free energy. We have shown that (i)–(iii) share the same formal root, and can be expressed as a freedom in the choice of a set of atomic weights $w_\kappa$. This choice should be made once and for all at the beginning, and consistently respected throughout the calculation of all free-energy coefficients; then, the physical answers that we extract from Eq. (1) should not depend on the specific set of $w_\kappa$ that we use. The variational solution of the continuum differential equations does depend, in general, on $w_\kappa$, but it must be this way: if we are asking, for example, "what is the local displacement of the cell at the point $\mathbf{r}$," the answer inevitably depends on how we define such a displacement via Eq. (37). Similar considerations hold whenever we use the information on $\mathbf{u}(\mathbf{r})$, extracted from experimental or theoretical domain-wall structures via Eq. (37), to estimate the flexocoupling coefficient by inverting Eq. (6).

## III. RESULTS

### A. Computational parameters

Our calculations are performed in the framework of DFT as implemented in the "in-house" LAUTREC code [32]. We use the local-density approximation [33], the projector augmented wave method (PAW) [34], and a plane-wave basis set with a kinetic energy cutoff of 50 Ry in all our calculations. The PAW datasets are generated by treating the following orbitals as valence electrons: Ba($5s^25p^66s^2$), Ca($3s^23p^64s^2$), K($3s^23p^64s^1$), Na($2s^22p^63s^1$), Nb($4s^24p^65s^24d^3$), O($2s^22p^4$), Pb($6s^25d^{10}6p^2$), Sr($4s^24p^65s^2$), Ti($3s^23p^64s^23d^2$), and Zr($4s^24p^65s^24d^2$). In all calculations, the Brillouin zone is sampled using Monkhorst-Pack [35] meshes that are equivalent (or better) to an $8\times8\times8$ $k$-point grid in the five-atom bulk cell.

For each of six $ABO_3$ perovskites ($BaTiO_3$, $CaTiO_3$, $KNbO_3$, $NaNbO_3$, $PbTiO_3$, and $PbZrO_3$) we first calculate the equilibrium lattice parameter $a_0$ of the cubic reference structure by fitting the energy to the Murnaghan equation of state. (The resulting values are listed in Table I.) Using the corresponding $a_0\times a_0\times a_0$ five-atom cells, we then displace the atoms along one of the main axes and reoptimize their positions, leading to tetragonal configurations with lower energy. The displacements from the cubic positions $d_\kappa$ and the energy differences $\Delta E$ and spontaneous polarization $P$ (calculated via the method of Ref. [36]) are reported in Table I. Based on the calculated values of $\Delta E$ and equilibrium polar distortion amplitude $P_0$, we then calculate $A$ and $B$ as

$$A=\frac{4\Delta E}{\Omega P_0^2},\qquad B=-\frac{4\Delta E}{\Omega P_0^4}. \tag{38}$$

In order to calculate the second-order term in the long-wave expansion of the force-constant matrix, Eq. (21), we use the real-space supercell approach of Ref. [21]. This implies calculating the second-order moments of the interatomic force constants according to

$$\Phi^{(2,xx)}_{\kappa y,\kappa' y}=\sum_l \Phi^l_{\kappa y,\kappa' y}(\mathbf{R}_l+\boldsymbol{\tau}_{\kappa'}-\boldsymbol{\tau}_\kappa)_x^2. \tag{39}$$

[Because of inversion symmetry, displacements of the atoms along $y$ do not generate electric fields along $x$; this implies that the interatomic forces decay exponentially with distance, and the lattice sums in Eq. (39) converge to a unique, well-defined value.] To compute $\Phi^l_{\kappa y,\kappa' y}$, we carry out calculations in which we displace one atom at the time by 0.005 a.u. along $y$ and extract the resulting forces. In practice, we use a $8a_0\times a_0\times a_0$ supercell, with the same geometry as in Fig. 2, except that we use the centrosymmetric paraelectric structure as reference. (The resulting matrix elements are given in Appendix A.)

Finally, to validate the model results against full DFT calculations, we prepare two domains with opposite polarization in a long (100)-oriented supercell (as in Fig. 2, for

TABLE I. Data computed using DFT for six perovskite oxides: simple-cubic lattice parameter $a_0$ (in Å); displacements (in Å) of the atoms from their high-symmetry positions in the distorted tetragonal structure at fixed lattice constants $a_0$, $d_\kappa$, for the $A$ cation ($d_A$), $B$ cation ($d_B$), apical anion ($d_{O_1}$), and equatorial anions ($d_{O_{2,3}}$); energy of this relaxed tetragonal configuration with respect to the simple cubic one (in meV/f.u.); and polarization of the tetragonal phase (in $C/m^2$). (*) indicates calculations of $BaTiO_3$ under hydrostatic pressure; see Sec. III D.

| | $a_0$ | $d_A$ | $d_B$ | $d_{O_1}$ | $d_{O_{2,3}}$ | $\Delta E$ | $P$ |
|---|---|---|---|---|---|---|---|
| $BaTiO_3$ | 3.935 | +0.0186 | +0.0538 | −0.0359 | −0.0183 | −2.87 | 0.188 |
| $BaTiO_3^{(*)}$ | 3.904 | +0.0087 | +0.0237 | −0.0117 | −0.0064 | −0.083 | 0.078 |
| $CaTiO_3$ | 3.799 | +0.2369 | +0.0584 | −0.0432 | −0.1261 | −36.72 | 0.508 |
| $KNbO_3$ | 3.947 | +0.0244 | +0.0553 | −0.0229 | −0.0287 | −3.77 | 0.205 |
| $NaNbO_3$ | 3.907 | +0.2097 | +0.0498 | −0.0480 | −0.1057 | −18.75 | 0.359 |
| $PbTiO_3$ | 3.879 | +0.1894 | +0.0793 | −0.0524 | −0.1081 | −30.56 | 0.578 |
| $PbZrO_3$ | 4.102 | +0.3674 | +0.0716 | −0.0241 | −0.2075 | −187.50 | 0.647 |

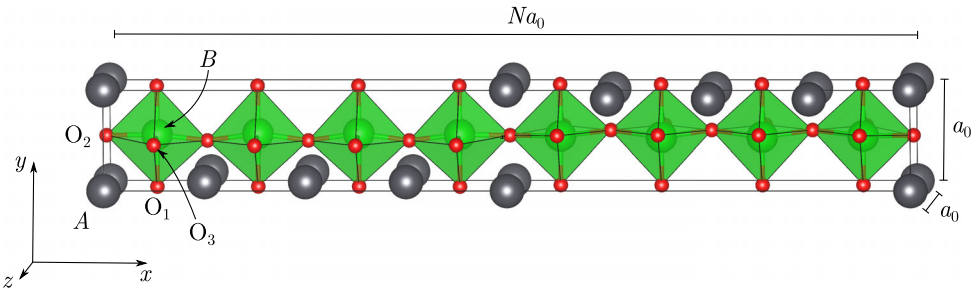


FIG. 2. Example of unit cell used in some of our full-DFT calculations (here, $N = 8$, and domains with opposite orientations give rise to an $AO$-type domain wall).

different values of $N$), and we allow the atoms to relax along $y$ till the forces on them are negligible. We consider both $AO$-centered and $BO_2$-centered wall types. Note that we neglect octahedra rotations, strain relaxations, or other wall orientations that might result in energetically more favorable structures. Our main goal here is testing the continuum approximation on a minimal Landau model of a ferroelectric wall, and discussing the subtleties related to the treatment of gradient effects. In this sense, incorporating additional degrees of freedom to achieve a more realistic picture would have constituted an unnecessary complication. In some members of our materials set such a simplified model does not yield a physically meaningful description of the bulk or domain-wall structure (or both). For this reason, we primarily focus our attention on $BaTiO_3$, $PbTiO_3$, and $KNbO_3$, and present the data on other materials for comparison purposes and future reference.

### B. DFT calculations of domain walls

We start by discussing our direct DFT calculation of the domain-wall structures. Figure 3 shows the resulting atomic displacements from the high-symmetry positions. Two features are common to all materials: the domain walls are atomically thin and the atomic positions at the center of each domain depend only on the material, and not on the type of wall ($AO$ or $BO_2$). The six oxides considered here can be roughly classified into two categories: those for which the relative displacement between $A$ cations in

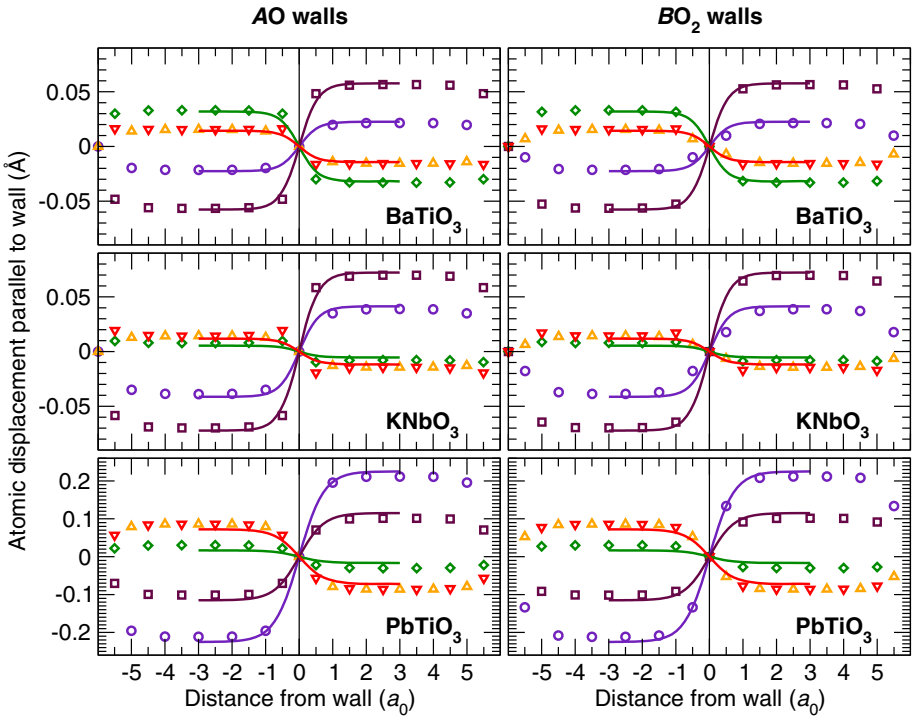


FIG. 3. Empty symbols: relaxed displacements of the atoms in the direction parallel to the domain wall as a function of the normal coordinate, extracted from full DFT calculations (circles, squares, diamonds, and triangles represent, respectively, $A$, $B$, apical O, and equatorial O atoms). Continuous curves: atomic displacement profiles predicted by the Landau model. Two possible types of domain wall (either $AO$- or $BO_2$-centered) are shown for three of the six perovskites considered in this work.

TABLE II. Domain-wall properties for six perovskite oxides: domain-wall energy $W$ as computed using DFT (for the two possible $AO$ and $BO_2$ domain walls) and as computed using the Landau model; and domain-wall thickness $\xi$ as computed using the Landau model.

| | $W$ (mJ/m$^2$) | | | $\xi$(Å) |
|---|---|---|---|---|
| | DFT ($AO$) | DFT ($BO_2$) | Eq. (12) | Eq. (10) |
| $BaTiO_3$ | 2.95 | 4.59 | 4.43 | 2.204 |
| $BaTiO_3^{(*)}$ | 0.321 | 0.322 | 0.324 | 5.441 |
| $CaTiO_3$ | 63.2 | 60.8 | 70.5 | 2.463 |
| $KNbO_3$ | 4.46 | 6.61 | 6.03 | 2.303 |
| $NaNbO_3$ | 26.6 | 32.7 | 34.3 | 2.557 |
| $PbTiO_3$ | 54.9 | 58.1 | 63.8 | 2.855 |
| $PbZrO_3$ | 200 | 133 | 252 | 2.170 |

adjacent domains is significantly larger than the one between $B$ cations ($CaTiO_3$, $NaNbO_3$, $PbTiO_3$, and $PbZrO_3$), and those for which this is not the case ($BaTiO_3$ and $KNbO_3$). Such an outcome reflects the bulk distortion patterns quoted in Table I, which indeed shows that $BaTiO_3$ and $KNbO_3$ have similar properties, e.g., regarding the small displacements of their $A$ cations. A similar classification also applies to the domain-wall energies, listed in Table II: for $BaTiO_3$ and $KNbO_3$ the domain-wall energies are significantly smaller than in other oxides (about one order of magnitude smaller than in $PbTiO_3$), with the $BO_2$-type wall energy approximately 50% higher than the $AO$-type value. In other oxides the energies are larger, and for both types of wall they are within 25% of each other. (The $BO_2$ type becomes favored for $CaTiO_3$ and $PbZrO_3$.) This picture is consistent with earlier calculations [37] in $PbTiO_3$ and $BaTiO_3$, even though in our calculations the relaxation of the cell parameters is not allowed.

The atomic configurations and energies of some perovskite oxide domain walls have been studied in the past using DFT-based methods. Padilla *et al.* [38] carried out a pioneering study on 180° domain walls in $BaTiO_3$ using an effective Hamiltonian built from DFT results; they reported that the walls are atomically thin and centered at the Ba atoms, consistent with our results, and that the domain-wall energies are of the order of 10 mJ/m$^2$. Full DFT studies of 180° domain walls in $PbTiO_3$, first by Pöykkö and Chadi [39] and later by Meyer and Vanderbilt [37], reached the same conclusion regarding thickness, and predicted domain-wall energies of 100 to 200 mJ/m$^2$. In this case, the most favorable domain walls are found to be centered on the Pb atoms, which is again consistent with our findings. To the best of our knowledge, Ref. [37] was the first to point out the geometrical offset of the atomic rows between the oppositely polarized domains; we discuss this point extensively in the next section.

More recent studies have revealed that surprises may be in store even in systems that were hitherto believed to be simple and well understood. A particularly illuminating example concerns the prediction of secondary Bloch-like components in $PbTiO_3$ [40]. The contribution of secondary (or coprimary) antiferrodistortive modes (involving rotations of the $O_6$ octahedra) to the domain-wall energy and structure has also been studied in selected cases [41,42]. These works clearly indicate that our Eq. (1) is too simplified to provide a realistic picture in many materials; a follow-up work is currently under way to generalize our model to more complex geometries and boundary conditions. Although experimental probing of the structure and energetics of ferroelectric domain walls is still challenging, by now the characterization methods are mature enough to allow for a meaningful comparison to theoretical results. For example, it is now widely accepted that domain walls in perovskite oxides can be atomically thin (see, for example, Ref. [43] and other references therein) as we have found here.

### C. Landau model calculations of domain walls

In this section we develop Landau models for each of our six perovskite oxides according to the guidelines specified earlier. We start from the calculated distortion pattern ($d_\kappa$) and energy gain ($\Delta E$) of the tetragonal ferroelectric phase, as reported in Table I. After processing the latter values via the procedure described in Secs. II C and II F, we readily obtain the values of $A$, $B$, and $p_\kappa$ for each bulk material. The gradient-mediated coefficients of the model ($C$, $f$, $G$) are then computed from $p_\kappa$ and the calculated $\Phi^{(2,xx)}_{\kappa y,\kappa' y}$ via Eq. (22). To illustrate our arguments, we use two different choices of weights for defining $p_\kappa$ (and hence the $A$, $B$, $f$, and $G$ parameters of the model), by setting $w_\kappa$ either to equal values or to the physical masses of the atoms. We shall compare the results and demonstrate their mutual consistency in the following.

In Table III we summarize our results for the calculated model parameters depending on the weight choice. As expected, all parameters (with the exception of the elastic coefficient) considerably differ between the equal-mass and the standard-mass convention. Recall that this difference is twofold. First, there is a trivial scale factor (proportional to some power of $P_0$) that is due to the normalization of the polar eigendisplacements $p_\kappa$. The present choice of measuring the polar order parameter via the norm (in length units) of the atomic distortion amplitude differs from the usual convention of macroscopic theories. To connect with the latter we provide in Table V (Appendix C) the same coefficients in SI units, where we have set $P_0$ to the spontaneous polarization of the bulk crystal, in C/m$^2$. In this case, the $A$ and $B$ coefficients agree between different choices of the weights, while a discrepancy remains in both $f$ and $G$. Such a dependence of $f$ and $G$ on the weight choice relates to the ambiguity in the definition of the center of mass, which is subtracted by construction from $p_\kappa$ via Eq. (34). As we said, either source of arbitrariness must

TABLE III. Coefficients of the Landau model of Eq. (1) computed from DFT calculations. The values are calculated by expressing both $u$ and $P$ fields in Bohr units of length. Then, $A$ is in $10^{-3}$ Ha bohr$^{-5}$; $B$ in $10^{-3}$ Ha bohr$^{-7}$; $f$, $G$, and $C$ are all in atomic units of pressure, i.e., $10^{-3}$ Ha bohr$^{-3}$. In the top block unit weights are used. In the bottom block physical atomic masses are used as weights.

| | $A$ | $B$ | $C$ | $f$ | $G$ |
|---|---|---|---|---|---|
| $BaTiO_3$ | −0.276 | 74.6 | 4.61 | −0.560 | 2.47 |
| $BaTiO_3^{(*)}$ | −0.0503 | 83.3 | 4.77 | −0.590 | 2.66 |
| $CaTiO_3$ | −0.219 | 3.29 | 3.47 | −0.861 | 2.59 |
| $KNbO_3$ | −0.322 | 77.8 | 3.27 | −1.62 | 3.86 |
| $NaNbO_3$ | −0.135 | 2.65 | 2.56 | −1.36 | 2.30 |
| $PbTiO_3$ | −0.234 | 4.79 | 3.45 | −1.06 | 3.73 |
| $PbZrO_3$ | −0.365 | 2.26 | 2.09 | −0.386 | 3.14 |
| $BaTiO_3$ | −0.448 | 195 | 4.61 | −3.82 | 7.04 |
| $BaTiO_3^{(*)}$ | −0.0801 | 212 | 4.77 | −3.86 | 7.35 |
| $CaTiO_3$ | −0.219 | 3.30 | 3.47 | −2.28 | 3.87 |
| $KNbO_3$ | −0.316 | 74.9 | 3.27 | −4.15 | 8.26 |
| $NaNbO_3$ | −0.215 | 6.72 | 2.56 | −2.60 | 5.14 |
| $PbTiO_3$ | −0.302 | 8.02 | 3.45 | −5.49 | 13.1 |
| $PbZrO_3$ | −0.431 | 3.14 | 2.09 | −2.75 | 7.24 |

have no impact on the physical results that we extract from the model—we use this criterion to validate the internal consistency of our theory.

As a first test of such a claim, we use the calculated values of the coefficients to compute the energy and the width of the domain walls following Eqs. (10) and (12). We find that the results are indeed consistent (to machine precision) between the two weight choices. Table II shows that the domain-wall energies extracted from the model are also consistent with the results of our full DFT calculations; the level of agreement is remarkable considering the simplicity of the Landau model. The wall width, in particular, is of the order of the cubic lattice parameter in all cases, which provides a rather difficult test for the continuum approximation. (The latter is expected to break down at length scales that are comparable with the lattice periodicity.) Note that the direct DFT calculations yield a marked dependence of the domain-wall energy on the wall location with respect to the underlying atomic structure; such a dependence is obviously missing within the continuum description.

Next, we compute the elastic displacement field by combining Eqs. (5) and (9):

$$u(x) = -\frac{f}{C}P(x) = -\frac{f}{C}P_0 \tanh\frac{x}{\xi}. \tag{40}$$

The resulting profile, shown in Fig. 4, drastically differs depending on the weight choice, but is in excellent agreement with the "local center of mass" that we extract from our explicit domain-wall calculations by using the same

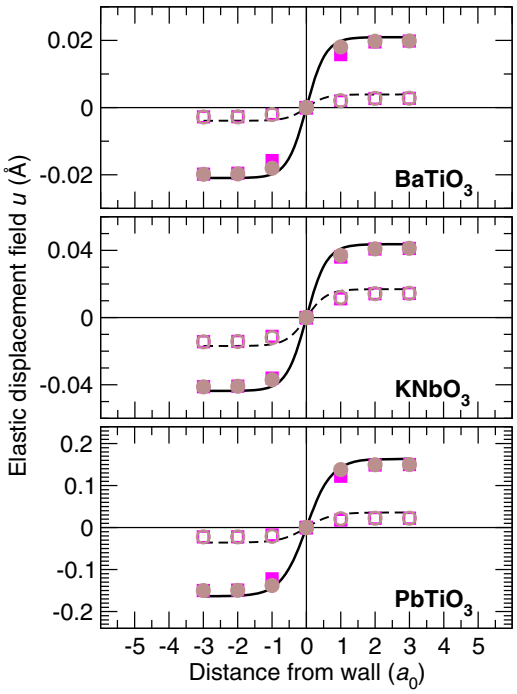


FIG. 4. Value of the elastic displacement field as a function of distance to the domain wall, for three perovskite oxides. The lines correspond to Landau model predictions using unit weights (broken lines) or atomic weights (continuous lines). The symbols correspond to local center-of-mass calculations computed with full DFT, for different cells centered on $AO$ or $BO_2$ layers, and for those two different weights.

weight convention. (For an $AO$ wall, we compute this by considering the positions of the $A$ and O atoms in a $AO$ layer together with an average of the $B$ and O atoms in adjacent $BO_2$ layers—we follow an equivalent procedure for the $BO_2$ walls.) In all materials considered here, taking unit weights (discontinuous lines) leads to flatter profiles than taking atomic weights (continuous lines), but with neither choice the centers of mass is fully aligned across the wall. Any choice of weights, on the other hand, leads to the same values of atomic displacements predicted by the Landau model via Eq. (13). The resulting curves are plotted as continuous lines next to the full DFT results for the domain-wall structures in Fig. 3. The agreement between the displacements predicted by the Landau model and those from full DFT calculations is obvious.

For a more quantitative analysis, we extract the overall displacement of the center of mass across the wall $\Delta u$ from the relaxed domain-wall structures, and use it to estimate the effective flexocoupling coefficient by inverting Eq. (6):

$$f^{\text{eff}} = -C\frac{\Delta u}{2P_0}. \tag{41}$$

The results for both choices of weights are compared in Table IV to the values predicted by the macroscopic model.

TABLE IV. Value of $f^{\text{eff}} = -C\Delta u/2P_0$, in V, as computed with DFT and with our Landau model. In the top block unit masses are used. In the bottom block actual atomic masses are used.

| | DFT ($AO$) | DFT ($BO_2$) | Landau model |
|---|---|---|---|
| $BaTiO_3$ | −0.203 | −0.198 | −0.283 |
| $BaTiO_3^{(*)}$ | −0.279 | −0.279 | −0.288 |
| $CaTiO_3$ | −0.409 | −0.454 | −0.681 |
| $KNbO_3$ | −0.676 | −0.670 | −0.793 |
| $NaNbO_3$ | −1.07 | −1.09 | −1.33 |
| $PbTiO_3$ | −0.395 | −0.400 | −0.628 |
| $PbZrO_3$ | 0.038 | −0.124 | −0.373 |
| $BaTiO_3$ | −1.43 | −1.43 | −1.52 |
| $BaTiO_3^{*}$ | −1.47 | −1.48 | −1.49 |
| $CaTiO_3$ | −1.53 | −1.57 | −1.80 |
| $KNbO_3$ | −1.93 | −1.92 | −2.05 |
| $NaNbO_3$ | −1.75 | −1.76 | −2.01 |
| $PbTiO_3$ | −2.63 | −2.64 | −2.87 |
| $PbZrO_3$ | −2.04 | −2.20 | −2.45 |

One can note that the equal-weight convention yields values of $f$ and $f^{\text{eff}}$ that are systematically smaller than those obtained by setting $w_\kappa$ to the physical atomic masses. Overall, the values of $f^{\text{eff}}$ and $f$ nicely agree, differing at most by few tenths of a volt in all cases.

Interestingly, the continuum approach yields a slight overestimation of the converse flexoelectric effect at the wall; such a feature appears to be systematic across all the materials set and irrespective of the weight convention being used. A possible explanation might lie in the atomically sharp nature of the domain-wall structures, which clearly challenges the continuum description. The estimated values of $f^{\text{eff}}$, however, appear to be largely insensitive to the atomistic details of the wall ($AO$- and $BO_2$-type walls yield very similar values for most materials); therefore, it is unlikely that the aforementioned discrepancy originates from the continuum approximation itself. We suspect that such an effect may depend on higher-order terms (either in the gradient expansion or in the polar distortion amplitude) that we neglect in Eq. (1). In any case, the accuracy of the present theory is more than sufficient for a quantitative comparison of first-principles calculations and experiments, e.g., along the lines of Ref. [13].

### D. "Soft" ferroelectric walls: $BaTiO_3$ under pressure

The values of $\xi$ in Table II are smaller than one lattice parameter in all cases, which agrees with the usual perception that 180° ferroelectric domain walls are very thin. In order to evaluate the accuracy of the polarization profile of Eq. (9) it would be desirable to study thicker ferroelectric domain walls with a smaller distortion amplitude; in such a limit we expect the free-energy functional of Eq. (1) to match the results of direct DFT calculations *exactly*. One way to access this regime consists in using an external parameter to bring the material closer to the phase transition. [The domain-wall thickness, also known as *correlation length*, diverges in a vicinity of a ferroelectric phase transition, because of the vanishing $A$ coefficient at the denominator of Eq. (10).] Temperature is the most obvious choice in an experimental context; this is, however, impractical in the context of direct DFT simulations. A simpler alternative consists in applying a hydrostatic pressure $p$ to our simulation cells; in many ferroelectrics, this results in a suppression of the ferroelectric instability already at moderate values of $p$, thus mimicking the effect of increasing temperature in real experiments.

We apply this strategy to $BaTiO_3$ by repeating all the calculations under hydrostatic pressure; the corresponding results are indicated in the tables with a (*) symbol. We find that, at a lattice constant of 99.2% of the equilibrium $a_0$ (see Table I), the $A$ parameter is still negative, but its absolute value is about an order of magnitude smaller (see Table III) than in standard conditions. Consistently, as the soft mode eigenvalue approaches zero the atomic displacements around the wall become smoother, and the value of $\xi$ increases to 5.441 Å. The profile of atomic displacements for these walls is shown in Fig. 5: the results of the Landau model (continuous lines; parameters are reported in Table III) are essentially in perfect agreement with the full DFT results in a $20a_0 \times a_0 \times a_0$ unit cell (symbols), both for the $AO$ and for the $BO_2$ types of domain wall. The agreement regarding domain-wall energy is also extremely

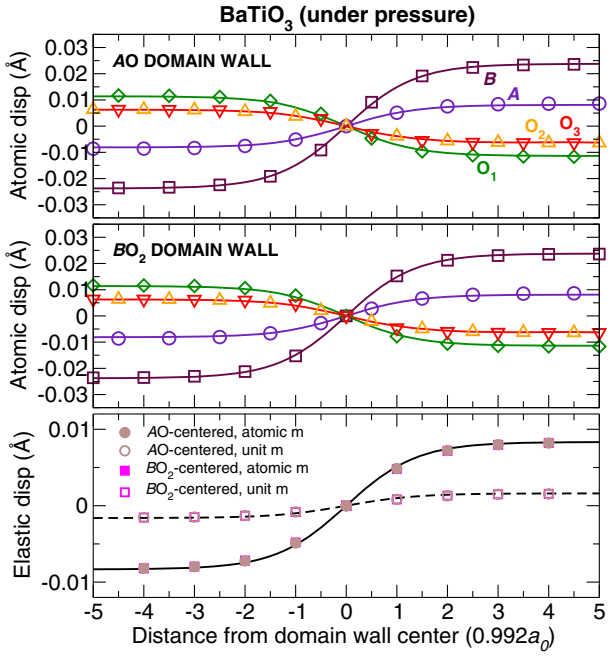


FIG. 5. Atomic displacements parallel to an $AO$ domain wall (top panel) and to a $BO_2$ wall (middle panel), and elastic displacement (bottom panel), as a function of the distance from the domain wall. In all cases the system studied is compressed $BaTiO_3$, built using supercells with a lattice parameter of $0.992a_0$.

good (see Table II): Equation (12) yields 0.324 $mJ/m^2$, while from full DFT calculations we obtain 0.321 $mJ/m^2$ (for the $AO$ type) and 0.322 $mJ/m^2$ (for the $BO_2$ type).

Note that the direct DFT calculations of the domain-wall energies and atomic structures are numerically much more challenging than in the zero pressure case, because of the extreme softness of the ferroelectric instability. To achieve a reasonable level of accuracy, and hence allow for a meaningful comparison to the model results, we had to be unusually careful with the usual computational parameters: (i) the domain-wall calculations were performed with a larger $20a_0 \times a_0 \times a_0$ unit cell, to accommodate the thicker wall structure, (ii) the five-atom unit cell calculations were done using a $20 \times 8 \times 8$ Monhkhorst-Pack grid, exactly reproducing the folded Brillouin zone of the supercell (the ferroelectric distortion amplitude and double-well potential depth is remarkably sensitive to the $\mathbf{k}$-point mesh), (iii) the tolerance on residual forces was set to 0.0001 eV/Å, approaching the inherent precision limits of the numerical algorithms. On the other hand, the calculation of the Landau model parameters required a similar computational effort as in the zero-pressure case, highlighting the obvious advantages of our multiscale approach in softer ferroic materials.

## IV. DISCUSSION

The impact of flexoelectricity on the properties of ferroelectric domain walls was studied in several recent works [12,13,44–46]. Yudin and Tagantsev [12] established the role of flexoelectricity in determining the elastic offset at the wall, as well as its impact on domain-wall energy and thickness via the renormalization of the polarization gradient coefficient $G$. These formal results, which we have largely built upon in our present work, were applied by Wang *et al.* [13] to domain-wall structures in $PbTiO_3$ that were obtained via either first-principles calculations or experimental microscopy images. These authors, however, assumed that an "authentic" [13] definition of the strain exists, and overlooked (as did earlier works on this topic) the inherent arbitrariness that we highlight here. The definition used by Ref. [13] corresponds to using physical masses as weights within our formalism. Within such a convention, however, our result of $f_{44} = -2.87$ V (or $f_{44}^{\mathrm{eff}} = -2.64$ V as extracted from the direct calculation of the $BO_2$-centered domain-wall structure) in $PbTiO_3$ disagrees with the value of $f_{44} = -5.4$ V quoted by Wang *et al.* by a factor of 2. We believe that the source of the disagreement lies in Eq. (9b) of Wang *et al.* [13], where an additional factor of 2 is indeed present compared to our Eq. (41). Note that our calculated $C = 101$ GPa is in excellent agreement with the value of $C_{44} = 100.8$ GPa quoted therein, ruling out possible issues in the definition of the shear elastic constant. Once the result of Ref. [13] is divided by 2, it is in excellent agreement with ours.

From the point of view of the physics, the main conceptual advance of our work can be summarized as follows. The contribution of flexoelectricity to the domain-wall properties is ill defined; however, the contribution of the polarization gradient energy is ill defined as well, and including both terms is essential for guaranteeing that their respective arbitrariness cancels out. The obvious question then is, is it really necessary to consider both terms explicitly? Or can we choose the weights in such a way that the contribution of flexoelectricity vanishes identically, leaving only the gradient terms? A quick glance at Fig. 4 suggests, at first sight, that the answer to the latter question be "yes": for the equal-weights case, the elastic offset between the domains is already small—by weighing the cations slightly less than the oxygens, one could certainly make $\Delta u$ to vanish exactly. However, this would "renormalize out" flexoelectricity only for a [100]-oriented wall; the same choice of weights would not yield a vanishing $\Delta u$ for a different (say, [110]) orientation. This means that, for a truly isotropic material, flexoelectricity can be reabsorbed into the polarization gradient energy, while anisotropic crystals generally require its explicit treatment. In other words, one can equivalently state that the renormalized gradient coefficients $\tilde{G}$ contain a *nonanalytic elastic contribution*, which generally prevents their representation in a straightworward tensorial form. This adds up to the more conventional sources of nonanaliticity, due to the long-range electrostatic interactions, which we have not covered in the present work. Interestingly, electrostatic and elastic interactions mediated by flexoelectricity share many similarities, as the former also enjoy a covariance principle [27] and become analytic (i.e., short-ranged) in isotropic media [27].

Another conceptual advance of this work consists in establishing a first-principles theory of the polarization gradient coefficient $G$. The established procedure to infer the value of $G$ from the phenomenological point of view consists in analyzing the dispersion of the phonon band associated with the soft mode [47]. The conceptual difficulties of defining $G$ in a microscopic context, and the often counterintuitive consequences of combining LGD models with density-functional theory, have been emphasized very recently [48]. (For example, an estimation based on the calculated spontaneous polarization and domain-wall energy resulted [48] in a large variation of $G$ as a function of the applied pressure.) In contrast with the results of Ref. [48], the $G$ coefficient as defined in our work changes little (2%–3% deviation for an isotropic compressive strain of 1%) with external pressure in $BaTiO_3$, consistent with the usual assumptions of LGD theory. This, together with the excellent accuracy of the domain-wall energies and structures calculated within our continuum approach, allows us to reach a more optimistic conclusion (compared to Ref. [48]) regarding the suitability of LGD equations for the description of realistic domain-wall structures.

Before closing, it is useful to place the methodology that we have developed here in the context of the existing

literature. Our strategy differs in spirit from Landau-Ginzburg-Devonshire theories in that the latter have been traditionally approached with a phenomenological mindset. Granted, combining first-principles techniques with LGD theories is not new: the former are being increasingly used [49] to estimate a subset, or even the entirety of the LGD model coefficients. However, such a practice is seldom supported by a formal link between the macroscopic and microscopic degrees of freedom, which has thwarted so far a quantitative validation of LGD models against the *ab initio* results. (At the qualitative level, successful comparisons do exist; see Ref. [45] for an example that is relevant to the topics of this work.) The conceptual novelty of our approach consists in deriving the macroscopic field equations as a rigorous long-wave approximation to the discrete lattice Hamiltonian. This constitutes a much more intimate synergy between the two levels of theory, which allows for quantitatively accurate predictions (compared to the "training" first-principles model) of the relevant physical properties. Most importantly, our approach leads to a deeper awareness of the internal structure of the theory, the mutual relation between the many physical quantities involved, and their potential dependence on some arbitrary choices that are inevitable in the mapping of the problem onto continuum fields.

For the above reasons, our "first-principles macroscopic theory" belongs to the class of methods that are commonly known as *second principles*. The latter are obtained via an appropriate coarse graining of the first-principles Hamiltonian, whose physically relevant low-energy degrees of freedom are treated explicitly, while most of the original complexity is integrated out. In the case of ferroelectrics, the reference in this context is the "effective Hamiltonian" method, pionereed by Zhong *et al.* [24]; many improvements and generalizations thereof have been introduced over the years [50,51]. Performing a fair comparison of the virtues and shortcomings of either strategy would require substantial additional work, and will be best carried out in the framework of a separate publication. Here we limit ourselves to observe that, once the continuum differential equations are discretized on a regular mesh corresponding to the unit cells of the original perovskite lattice, our approach essentially reduces to an effective Hamiltonian—at least for the simple domain-wall geometry considered here. [A generalization to the full three-dimensional case appears feasible, too, by writing all the couplings of Eq. (1) in a tensorial form and by explicitly treating the electrostatic energy.] From this point of view, the present method effectively bridges the gap between atomistic and continuum approaches, while preserving an exact limit at length scales that are large compared to the interatomic spacings.

## V. CONCLUSIONS

We have established a formal mapping between continuum fields and atomistics, and demonstrated its predictive power in the study of spatially inhomogeneous structures (e.g., domain walls) in ferroics. Our formalism demonstrates the necessity of abandoning some widespread beliefs in continuum theory, for example, that the local strain field be a physically well-defined degree of freedom of the crystal. While the arbitrariness in the definition of the elastic strain has a profound impact on the continuum model coefficients, we demonstrate that the physical answers derived from the model are robust against the specific convention that is being used.

On one hand, this results in a fundamental *principle of invariance* that we deem of great practical utility in validating the internal consistency of the continuum equations. On the other hand, and most importantly, our results provide a stringent benchmark to determine what are the physically sound questions that one can ask, and what are not. As illustrated by our practical tests, examples of well-posed questions concern the domain-wall energy, or the atomic positions; we show that macroscopic theory (within the validity range of the continuum approximation) can be an excellent tool to predict both—with comparable accuracy to the full first-principles "training model." Conversely, questions of the type "what is the contribution of flexoelectricity to the domain-wall energy?" or "what is the impact of the dynamic flexoelectric effect on the acoustic phonon dispersion?" are physically meaningless, as the answer can be about "anything," depending on some (necessarily) arbitrary choices that one makes along the way.

In the present work we have voluntarily chosen, for the sake of clarity, a minimal model of macroscopic phenomena where the above ideas have a nontrivial impact. (For example, we have neglected most components of the strain tensor, as well as competing antiferrodistortive modes.) This choice has inevitably limited the predictive power of our study in some materials. An obvious future development of this work consists in extending the scopes of our first-principles continuum approach to more complex structures, e.g., involving a higher dimensionality or a broader range of degrees of freedom. For example, it will be interesting to clarify whether the principle of invariance established here also applies to the bichiral domain-wall structures described in Refs. [44,45], or to the secondary Bloch-like components that were theoretically predicted in $PbTiO_3$ [40]. Also, incorporating the effect of octahedral tilts appears especially promising, in light of the results of Ref. [10]. Generalizing the ideas developed here in such directions will be an exciting avenue for further study.

## ACKNOWLEDGMENTS

O. D. acknowledges funding from the Israel Science Foundation under Grants No. 1814/14 and No. 2143/14. M. S. acknowledges the support of Ministerio de Ciencia e Innovación (MICINN-Spain) through Grant No. PID2019–108573 GB-C22 and Severo Ochoa FUNFUTURE center

of excellence (CEX2019-000917-S), of Generalitat de Catalunya (Grant No. 2017 SGR1506), and of the European Research Council (ERC) under the European Union's Horizon 2020 research and innovation program (Grant Agreement No. 724529).

## APPENDIX A: RELATION TO THE EIGENMODE REPRESENTATION

In this appendix, we shall link the formalism developed in the main text to the prescriptions of Ref. [27] for the construction of the continuum Hamiltonian. Their proposed strategy consists in identifying the distortion patterns associated with the mechanical displacement and polarization fields with, respectively, the acoustic and "soft" polar eigenmodes of the zone-center dynamical matrix $\mathcal{D}$. We adopt here a slightly more general definition by introducing the following operator,

$$\tilde{\mathcal{D}}_{\kappa\alpha,\kappa'\beta} = \frac{1}{\sqrt{w_\kappa w_{\kappa'}}} \Phi^{(0)}_{\kappa\alpha,\kappa'\beta}, \tag{A1}$$

which reduces to the standard definition of $\mathcal{D}$ when the weights are set to the physical atomic masses $m_\kappa$. (In our formalism the weights are dimensionless, so the appropriate choice in this case consists in setting them to the *fractional* mass of the sublattice; then, $\tilde{\mathcal{D}}$ reduces to $M_{\text{tot}}\mathcal{D}$, where $M_{\text{tot}} = \sum_\kappa m_\kappa$ is the total mass of the cell.) Following Ref. [27], we define the eigendisplacement pattern $|\nu\alpha\rangle$ associated to a given normal mode $\nu\alpha$ ($\nu$ runs over the four $T_{1u}$ irreps of the cubic perovskite structure, including acoustic and optical $\text{TO}_1$–$\text{TO}_3$ modes; $\alpha$ is a Cartesian direction) as

$$\langle\kappa\beta|\nu\alpha\rangle = \sqrt{\frac{1}{w_\kappa}}\langle\kappa\beta|v^{(\nu)}_\alpha\rangle, \tag{A2}$$

where $|v^{(\nu)}_\alpha\rangle$ are the normalized eigenvectors of $\tilde{\mathcal{D}}$. (The present use of the bra-ket notation follows the conventions established in earlier works [27,28]. Both bras and kets are real vectors in a space of dimension $3N_{\text{at}}$, where $N_{\text{at}}$ is the total number of atoms in the unit cell; $\langle\kappa\beta|$ form a complete orthonormal basis.) This definition results in a generalized orthonormality condition for the eigendisplacements,

$$\langle\nu\alpha|W|\nu'\beta\rangle = \delta_{\nu\nu'}\delta_{\alpha\beta}, \tag{A3}$$

where the "overlap operator" $W$ is defined as

$$W_{\kappa\alpha,\kappa'\beta} = w_\kappa\delta_{\kappa\kappa'}\delta_{\alpha\beta}. \tag{A4}$$

One can show [27] that, within such prescriptions, the eigendisplacements associated to the acoustic mode ($\nu = u$) are independent of the weights, thus recovering Eq. (16). Then, by setting $\nu = u$ and $\nu' = \text{TO}_1$–$\text{TO}_3$ in Eq. (A3), we find that both Eqs. (34) and (34b) are automatically satisfied by all polar modes. We can, thus, identify the symbol $\langle\kappa\beta|\nu\alpha\rangle$ with the transformation matrix introduced in Sec. II C:

$$\langle\kappa\beta|\nu\alpha\rangle = T_{\kappa\beta,\nu\alpha}. \tag{A5}$$

In particular, the elastic displacement and polarization basis vectors are defined by

$$\langle\kappa\beta|u\alpha\rangle = \delta_{\alpha\beta}, \qquad \langle\kappa\beta|\text{TO}_1\alpha\rangle = \delta_{\alpha\beta}p^{(\alpha)}_\kappa, \tag{A6}$$

where we have assumed that $\text{TO}_1$ corresponds to the ferroelectric "soft mode."

There is a slight drawback with such a procedure: different conventions for the weights lead to definitions of $p^{(\alpha)}_\kappa$ that are generally not related via Eq. (25). Indeed, the configuration space spanned by $p^{(\alpha)}_\kappa$ changes depending on the weights, as the three polar optical modes of the perovskite structure can mix. (This is a well-known issue in the construction of effective Hamiltonian for ferroelectrics, where typically the lowest eigenvector of the force-constant matrix is used for $p^{(\alpha)}_\kappa$; this corresponds to choosing equal weights in the context of our formalism.) In practical cases, $p^{(\alpha)}_\kappa$ might not reproduce the correct distortion pattern (and energetics) of the bulk ferroelectric ground state, which is undesirable in the study of a domain wall. To avoid this issue, in this work we have followed the prescriptions of Sec. II F and defined $p^{(\alpha)}_\kappa$ starting from the relaxed distortion pattern of the bulk ferroelectric crystal instead. In the limit of a weak ferroelectric instability, one can show that this definition of $p^{(\alpha)}_\kappa$ exactly matches the eigenvector representation provided by Eq. (A6) regardless of the choice of the weights.

## APPENDIX B: DYNAMICAL EQUATIONS OF MOTION

Tagantsev [52] and Kvasov and Tagantsev [53] claimed that there are two well-defined contributions to the bulk flexoelectric tensor, static and dynamic in nature, and that they are, in principle, separately measurable. Later works [22] clarified that such a partition is arbitrary, and that (i) the total flexoelectric coefficient is meaningful for dynamical problems and (ii) either the total or the "static" flexoelectric tensor yield identical answers at mechanical equilibrium. To firm up our arguments, we shall revisit this long-standing debate on the static versus dynamic contribution to the flexoelectric tensor in light of the results presented so far. We shall see that it bears strong connections to the aforementioned ambiguities in the definitions of the continuum fields, and that our formalism resolves once and for all the existing confusion around this topic. The coupled dynamics of the polar and acoustic

degrees of freedom is, of course, irrelevant to the study of static structures, such as the domain walls that we consider in this work. Still, it is interesting to discuss this topic here, as it provides an additional proof of the internal consistency of our arguments.

To describe the dynamical evolution of the mechanical and acoustic degrees of freedom, we need to work out the kinetic energy density in terms of the mode velocities. We shall write it as

$$\mathcal{T}(\mathbf{r}) = \frac{1}{2}\sum_{\nu\nu'\alpha\beta} \dot{v}_{\nu\alpha}(\mathbf{r}) M_{\nu\alpha,\nu'\beta} \dot{v}_{\nu'\beta}(\mathbf{r}), \tag{B1}$$

where $\alpha\beta$ run over all the Cartesian components of the vector fields indexed by $\nu\nu'$, and the matrix $M_{\nu\alpha,\nu'\beta}$, of the dimension of a mass density, is the normal mode representation of the "mass operator" $M$:

$$M_{\nu\alpha,\nu'\beta} = \frac{1}{\Omega}\langle \nu\alpha | M | \nu'\beta \rangle,$$
$$\langle \kappa\alpha | M | \kappa'\beta \rangle = m_\kappa \delta_{\kappa\kappa'}\delta_{\alpha\beta}. \tag{B2}$$

(As usual, $\kappa\kappa'$ are sublattice indices; $m_\kappa$ are atomic masses.) The off-diagonal kinetic term, coupling the acoustic and optical mode velocities, has been identified as a *dynamical* contribution to the bulk flexoelectric tensor by Tagantsev and co-workers [12,52,53].

Based on the arguments of the earlier sections, it is clear that the magnitude of such contribution, and even whether it exists at all, depends on the choice we make for the weights $w_\kappa$. The definition given by Tagantsev of the "static" flexoelectric tensor corresponds, within our formalism, to using equal weights in the construction of our free-energy functional coefficients. If we do so, the matrix element $M_{uP}$ then reduces to their definition of the "dynamic" contribution. If we made a different choice, the partition between the two would change arbitrarily—and yet both the dynamical (phonon frequencies and dispersions) and static properties (domain-wall energy, equilibrium atomic positions) predicted by our Lagrangian would be *exactly* the same. It is interesting to consider the special case where the weights are set to the physical masses of the atoms divided by the total mass of the cell, $w_\kappa = m_\kappa/(\sum_{\kappa'} m_{\kappa'})$. The orthogonality condition, Eq. (A3), immediately leads then to $M_{uP} = 0$; i.e., the "dynamical flexoelectric effect" disappears altogether. Given that the magnitude, and even the very existence, of such an effect depends on some arbitrary convention we have made along the way in order to map our lattice-dynamical problem onto a continuum Lagrangian density, we are forced to conclude that such an effect is not measurable. Still, we find that incorporating a mass cross term, as suggested in Ref. [12], is necessary to guarantee that the physical predictions of the theory are unaffected by such ambiguities.

## APPENDIX C: SUPPORTING NUMERICAL DATA

In Table V we provide the complete list of the calculated model coefficients for all materials. This is essentially the same data as in Table III, only expressed in SI units while setting $P_0$ to the spontaneous ferroelectric polarization of the bulk crystal. This conversion is useful for two purposes. First, it shows that the $A$ and $B$ coefficients are consistent between different weight choices, provided that the respective distortion vectors $p_\kappa$ are related via Eq. (25); i.e., they only differ by a sublattice-independent constant. [This is obviously the case if the electrical polarization is chosen as

TABLE V. Coefficients (in SI units) of the Landau model of Eq. (1) computed from DFT calculations, when $P_0$ is the spontaneous polarization of the bulk crystal (measured in $C/m^2$). In the top block unit weights are used. In the bottom block physical atomic masses are used.

| | $A$ ($10^9$ m/F) | $B$ ($10^{10}$ $\Omega^2$ m$^3$/kg) | $C$ ($10^{11}$ Pa) | $f$ (V) | $G$ ($10^{-10}$ m$^3$/F) | $\tilde{G}$ ($10^{-10}$ m$^3$/F) |
|---|---|---|---|---|---|---|
| $BaTiO_3$ | −0.857 | 2.43 | 1.36 | −0.283 | 0.214 | 0.208 |
| $BaTiO_3^{(*)}$ | −0.145 | 2.36 | 1.40 | −0.288 | 0.221 | 0.215 |
| $CaTiO_3$ | −1.66 | 0.645 | 1.02 | −0.681 | 0.550 | 0.505 |
| $KNbO_3$ | −0.934 | 2.22 | 0.961 | −0.793 | 0.313 | 0.248 |
| $NaNbO_3$ | −1.56 | 1.21 | 0.755 | −1.33 | 0.746 | 0.510 |
| $PbTiO_3$ | −1.00 | 0.299 | 1.01 | −0.628 | 0.447 | 0.409 |
| $PbZrO_3$ | −4.15 | 0.991 | 0.616 | −0.373 | 1.00 | 0.979 |
| $BaTiO_3$ | −0.857 | 2.43 | 1.36 | −1.52 | 0.378 | 0.208 |
| $BaTiO_3^{(*)}$ | −0.145 | 2.36 | 1.40 | −1.49 | 0.373 | 0.215 |
| $CaTiO_3$ | −1.66 | 0.645 | 1.02 | −1.80 | 0.822 | 0.505 |
| $KNbO_3$ | −0.934 | 2.22 | 0.961 | −2.05 | 0.684 | 0.248 |
| $NaNbO_3$ | −1.56 | 1.21 | 0.755 | −2.01 | 1.05 | 0.510 |
| $PbTiO_3$ | −1.00 | 0.299 | 1.01 | −2.87 | 1.22 | 0.409 |
| $PbZrO_3$ | −4.15 | 0.991 | 0.616 | −2.45 | 1.95 | 0.979 |

TABLE VI. Elements of the second-moment interatomic force-constant matrix (in atomic units), as computed using DFT calculations in 40-atom $8a_0 \times a_0 \times a_0$ unit cells, for six perovskite oxides.

| | $\Phi^{(2,xx)}$ | | | | |
|---|---|---|---|---|---|
| $BaTiO_3$ | 0.0920 | −0.5561 | −0.2022 | −0.0383 | −0.1299 |
| | −0.5561 | −0.0191 | 0.0539 | −0.0259 | −0.0202 |
| | −0.2022 | 0.0539 | −0.0847 | −0.7573 | 0.0142 |
| | −0.0383 | −0.0258 | −0.7573 | −0.4640 | 0.1104 |
| | −0.1299 | −0.0202 | 0.0142 | 0.1104 | −0.2174 |
| $BaTiO_3^{(*)}$ | 0.0915 | −0.5773 | −0.1854 | −0.0319 | −0.1605 |
| | −0.5773 | −0.0230 | 0.0580 | 0.0177 | −0.0231 |
| | −0.1854 | 0.0580 | −0.0799 | −0.7699 | 0.0142 |
| | −0.0319 | 0.0178 | −0.7699 | −0.4921 | 0.1119 |
| | −0.1605 | −0.0231 | 0.0142 | 0.1119 | −0.2326 |
| $CaTiO_3$ | 0.0082 | −0.3563 | −0.1513 | −0.0596 | 0.1967 |
| | −0.3563 | −0.0374 | 0.1251 | 0.2363 | −0.0124 |
| | −0.1513 | 0.1252 | −0.1968 | −0.9531 | 0.0092 |
| | −0.0596 | 0.2363 | −0.9531 | −0.7121 | 0.1835 |
| | 0.1967 | −0.0124 | 0.0092 | 0.1835 | −0.0636 |
| $KNbO_3$ | 0.0195 | −0.3345 | −0.1154 | −0.0194 | −0.0530 |
| | −0.3345 | −0.0671 | 0.1619 | 0.2763 | −0.0216 |
| | −0.1154 | 0.1619 | −0.1782 | −0.9074 | 0.0163 |
| | −0.0194 | 0.2763 | −0.9075 | −0.7123 | 0.1230 |
| | −0.0530 | −0.0216 | 0.0163 | 0.1230 | −0.0259 |
| $NaNbO_3$ | 0.0022 | −0.2023 | −0.0782 | −0.0274 | 0.0916 |
| | −0.2023 | −0.0821 | 0.2043 | 0.3915 | −0.0237 |
| | −0.0782 | 0.2043 | −0.2783 | −0.9913 | 0.0250 |
| | −0.0274 | 0.3916 | −0.9913 | −0.8334 | 0.1769 |
| | 0.0916 | −0.0237 | 0.0250 | 0.1769 | −0.0063 |
| $PbTiO_3$ | −0.0529 | −0.3944 | −0.0856 | −0.0003 | 0.1969 |
| | −0.3944 | −0.0254 | 0.0977 | 0.1092 | −0.0240 |
| | −0.0856 | 0.0978 | −0.1416 | −0.7698 | −0.0300 |
| | −0.0003 | 0.1092 | −0.7698 | −0.4886 | 0.0226 |
| | 0.1969 | −0.0240 | −0.0300 | 0.0226 | −0.2507 |
| $PbZrO_3$ | −0.1344 | −0.3815 | −0.1047 | 0.0158 | 0.3713 |
| | −0.3815 | 0.0260 | 0.0573 | 0.1440 | −0.0367 |
| | −0.1047 | 0.0573 | −0.1189 | −0.5866 | −0.0134 |
| | 0.0158 | 0.1440 | −0.5866 | −0.5552 | 0.0543 |
| | 0.3713 | −0.0367 | −0.0134 | 0.0543 | −0.2071 |

a measure of the atomic distortion, but not when the total norm of the distortion is used; in the latter case there is generally an overall scaling factor that originates from Eq. (34b).] Second, the coefficients are now expressed in the same units as in conventional macroscopic theory, allowing for a direct comparison. In the case of $BaTiO_3$, for example, our calculated polarization gradient coefficient $G$ is in good agreement with the phenomenological value of $G = 0.2 \times 10^{-10}$ $m^3/F$ reported in Ref. [45].

The elements of the second-moment interatomic force-constant matrix, calculated via Eq. (39), are reported in Table VI for reference.


[1] J. Seidel, *Topological Structures in Ferroic Materials* (Springer, Cham, 2016), p. 826.

[2] Shanquan Chen, Shuai Yuan, Zhipeng Hou, Yunlong Tang, Jinping Zhang, Tao Wang, Kang Li, Weiwei Zhao, Xingjun Liu, Lang Chen, Lane W. Martin, and Zuhuang Chen, *Recent Progress on Topological Structures in Ferroic Thin Films and Heterostructures*, Adv. Mater. **33**, 2000857 (2021).

[3] P. Zubko, G. Catalan, and A. K. Tagantsev, *Flexoelectric Effect in Solids*, Annu. Rev. Mater. Res. **43**, 387 (2013).

[4] G. Catalan, A. Lubk, A. H. G. Vlooswijk, E. Snoeck, C. Magen, A. Janssens, G. Rispens, G. Rijnders, D. H. A. Blank, and B. Noheda, *Flexoelectric Rotation of Polarization in Ferroelectric Thin Films*, Nat. Mater. **10**, 963 (2011).

[5] H. Lu, C.-W. Bark, D. Esque de los Ojos, J. Alcala, C. B. Eom, G. Catalan, and A. Gruverman, *Mechanical Writing of Ferroelectric Polarization*, Science **336**, 59 (2012).

[6] L. E. Cross, *Flexoelectric Effects: Charge Separation in Insulating Solids Subjected to Elastic Strain Gradients*, J. Mater. Sci. **41**, 53 (2006).

[7] J. D. Axe, J. Harada, and G. Shirane, *Anomalous Acoustic Dispersion in Centrosymmetric Crystals with Soft Optic Phonons*, Phys. Rev. B **1**, 1227 (1970).

[8] Henning Pttker and Ekhard K. H. Salje, *Flexoelectricity, Incommensurate Phases and the Lifshitz Point*, J. Phys. Condens. Matter **28**, 075902 (2016).

[9] A. K. Tagantsev, K. Vaideeswaran, S. B. Vakhrushev, A. V. Filimonov, R. G. Burkovsky, A. Shaganov, D. Andronikova, A. I. Rudskoy, A. Q. R. Baron, H. Uchiyama, D. Chernyshov, A. Bosak, Z. Ujma, K. Roleder, A. Majchrowski, J. H. Ko, and N. Setter, *The Origin of Antiferroelectricity in* $PbZrO_3$, Nat. Commun. **4**, 2229 (2013).

[10] Andrea Schiaffino and Massimiliano Stengel, *Macroscopic Polarization from Antiferrodistortive Cycloids in Ferroelastic* $SrTiO_3$, Phys. Rev. Lett. **119**, 137601 (2017).

[11] Ekhard K. H. Salje, Suzhi Li, Massimiliano Stengel, Peter Gumbsch, and Xiangdong Ding, *Flexoelectricity and the Polarity of Complex Ferroelastic Twin Patterns*, Phys. Rev. B **94**, 024114 (2016).

[12] P. V. Yudin and A. K. Tagantsev, *Fundamentals of Flexoelectricity in Solids*, Nanotechnology **24**, 432001 (2013).

[13] Y. J. Wang, Y. L. Tang, Y. L. Zhu, Y. P. Feng, and X. L. Ma, *Converse Flexoelectricity around Ferroelectric Domain Walls*, Acta Mater. **191**, 158 (2020).

[14] R. Resta, *Towards a Bulk Theory of Flexoelectricity*, Phys. Rev. Lett. **105**, 127601 (2010).

[15] J. Hong, G. Catalan, J. F. Scott, and E. Artacho, *The Flexoelectricity of Barium and Strontium Titanates from First Principles*, J. Phys. Condens. Matter **22**, 112201 (2010).

[16] Miquel Royo and Massimiliano Stengel, *First-Principles Theory of Spatial Dispersion: Dynamical Quadrupoles and Flexoelectricity*, Phys. Rev. X **9**, 021050 (2019).

[17] Miquel Royo and Massimiliano Stengel, *Lattice-Mediated Bulk Flexoelectricity from First Principles*, Phys. Rev. B **105**, 064101 (2022).

[18] X. Gonze *et al.*, ABINIT: *First-Principles Approach to Material and Nanosystem Properties*, Comput. Phys. Commun. **180**, 2582 (2009).

[19] Aldo H. Romero *et al.*, ABINIT: *Overview and Focus on Selected Capabilities*, J. Chem. Phys. **152**, 124102 (2020).

[20] Q. Li, C. T. Nelson, S. L. Hsu, A. R. Damodaran, L. L. Li, A. K. Yadav, M. McCarter, L. W. Martin, R. Ramesh, and S. V. Kalinin, *Quantification of Flexoelectricity in* $PbTiO_3/SrTiO_3$ *Superlattice Polar Vortices Using Machine Learning and Phase-Field Modeling*, Nat. Commun. **8**, 1468 (2017).

[21] J. Hong and D. Vanderbilt, *First-Principles Theory and Calculation of Flexoelectricity*, Phys. Rev. B **88**, 174107 (2013).

[22] M. Stengel, *Flexoelectricity from Density-Functional Perturbation Theory*, Phys. Rev. B **88**, 174106 (2013).

[23] W. Zhong, David Vanderbilt, and K. M. Rabe, *Phase Transitions in* $BaTiO_3$ *from First Principles*, Phys. Rev. Lett. **73**, 1861 (1994).

[24] W. Zhong, David Vanderbilt, and K. M. Rabe, *First-Principles Theory of Ferroelectric Phase Transitions for Perovskites: The Case of* $BaTiO_3$, Phys. Rev. B **52**, 6301 (1995).

[25] Ph. Ghosez and K. M. Rabe, *Microscopic Model of Ferroelectricity in Stress-Free* $PbTiO_3$ *Ultrathin Films*, Appl. Phys. Lett. **76**, 2767 (2000).

[26] Igor A. Kornev, S. Lisenkov, R. Haumont, B. Dkhil, and L. Bellaiche, *Finite-Temperature Properties of Multiferroic* $BiFeO_3$, Phys. Rev. Lett. **99**, 227602 (2007).

[27] Massimiliano Stengel, *Unified Ab Initio Formulation of Flexoelectricity and Strain-Gradient Elasticity*, Phys. Rev. B **93**, 245107 (2016).

[28] Asier Zabalo and Massimiliano Stengel, *Switching a Polar Metal via Strain Gradients*, Phys. Rev. Lett. **126**, 127601 (2021).

[29] Max Born and Kun Huang, *Dynamical Theory of Crystal Lattices* (Oxford University Press, Oxford, 1954).

[30] A. Baldereschi, S. Baroni, and R. Resta, *Band Offsets in Lattice-Matched Heterojunctions: A Model and First-Principles Calculations for GaAs/AlAs*, Phys. Rev. Lett. **61**, 734 (1988).

[31] J. Junquera, M. H. Cohen, and K. M. Rabe, *Nanoscale Smoothing and the Analyis of Interfacial Charge and Dipolar Densities*, J. Phys. Condens. Matter **19**, 213203 (2007).

[32] LAUTREC is a massively parallel "in-house" electronic-structure code currently maintained by M. Stengel.

[33] J. P. Perdew and Y. Wang, *Accurate and Simple Analytic Representation of the Electron-Gas Correlation Energy*, Phys. Rev. B **45**, 13244 (1992).

[34] P. E. Blöchl, *Projector Augented-Wave Method*, Phys. Rev. B **50**, 17953 (1994).

[35] H. J. Monkhorst and J. D. Pack, *Special Points for Brillouin-Zone Integrations*, Phys. Rev. B **13**, 5188 (1976).

[36] M. Stengel and N. A. Spaldin, *Accurate Polarization within a Unified Wannier Function Formalism*, Phys. Rev. B **73**, 075121 (2006).

[37] B. Meyer and David Vanderbilt, *Ab Initio Study of Ferroelectric Domain Walls in* $PbTiO_3$, Phys. Rev. B **65**, 104111 (2002).

[38] J. Padilla, W. Zhong, and D. Vanderbilt, *First-Principles Investigation of 180° Domain Walls in* $BaTiO_3$, Phys. Rev. B **53**, R5969 (1996).

[39] S. Pykk and D. J. Chadi, *Ab Initio Study of 180° Domain Wall Energy and Structure in* $PbTiO_3$, Appl. Phys. Lett. **75**, 2830 (1999).

[40] Jacek C. Wojdeł and Jorge Íñiguez, *Ferroelectric Transitions at Ferroelectric Domain Walls Found from First Principles*, Phys. Rev. Lett. **112**, 247603 (2014).

[41] Axel Lubk, S. Gemming, and N. Spaldin, *First-Principles Study of Ferroelectric Domain Walls in Multiferroic Bismuth Ferrite*, Phys. Rev. B **80**, 104110 (2009).

[42] Oswaldo Diguez, Pablo Aguado-Puente, Javier Junquera, and Jorge Iniguez, *Domain Walls in a Perovskite Oxide with Two Primary Structural Order Parameters: First-Principles Study of* $BiFeO_3$, Phys. Rev. B **87**, 024102 (2013).

[43] Donald M. Evans, Vincent Garcia, Dennis Meier, and Manuel Bibes, *Domains and Domain Walls in Multiferroics*, Phys. Sci. Rev. **5**, 20190067 (2020).

[44] P. V. Yudin, A. K. Tagantsev, E. A. Eliseev, A. N. Morozovska, and N. Setter, *Bichiral Structure of Ferroelectric Domain Walls Driven by Flexoelectricity*, Phys. Rev. B **86**, 134102 (2012).

[45] Yijia Gu, Menglei Li, Anna N. Morozovska, Yi Wang, Eugene A. Eliseev, Venkatraman Gopalan, and Long-Qing Chen, *Flexoelectricity and Ferroelectric Domain Wall Structures: Phase-Field Modeling and DFT Calculations*, Phys. Rev. B **89**, 174111 (2014).

[46] Bo Wang, Yijia Gu, Shujun Zhang, and Long-Qing Chen, *Flexoelectricity in Solids: Progress, Challenges, and Perspectives*, Prog. Mater. Sci. **106**, 100570 (2019).

[47] J. Hlinka and P. Márton, *Phenomenological Model of a 90° Domain Wall in* $BaTiO_3$*-Type Ferroelectrics*, Phys. Rev. B **74**, 104104 (2006).

[48] Atanu Samanta, Suhas Yadav, Zongquan Gu, Cedric J. G. Meyers, Liyan Wu, Dongfang Chen, Shishir Pandya, Robert A. York, Lane W. Martin, Jonathan E. Spanier, and Ilya Grinberg, *A Predictive Theory for Domain Walls in Oxide Ferroelectrics Based on Interatomic Interactions and Its Implications for Collective Material Properties*, Adv. Mater. **34**, 2106021 (2022).

[49] Sergey Artyukhin, Kris T. Delaney, Nicola A. Spaldin, and Maxim Mostovoy, *Landau Theory of Topological Defects in Multiferroic Hexagonal Manganites*, Nat. Mater. **13**, 42 (2014).

[50] Jacek C. Wojdeł, Patrick Hermet, Mathias P. Ljungberg, Philippe Ghosez, and Jorge Íñiguez, *First-Principles Model Potentials for Lattice-Dynamical Studies: General Methodology and Example of Application to Ferroic Perovskite Oxides*, J. Phys. Condens. Matter **25**, 305401 (2013).

[51] Philippe Ghosez and Javier Junquera, *Modeling of Ferroelectric Oxide Perovskites: From First to Second Principles*, Annu. Rev. Condens. Matter Phys. **13**, 325 (2022).

[52] A. K. Tagantsev, *Piezoelectricity and Flexoelectricity in Crystalline Dielectrics*, Phys. Rev. B **34**, 5883 (1986).

[53] Alexander Kvasov and Alexander K. Tagantsev, *Dynamic Flexoelectric Effect in Perovskites from First-Principles Calculations*, Phys. Rev. B **92**, 054104 (2015).